Currents and transport on the Eastern Bering Sea shelf: An integration of over 20 years of data

P. J. Stabeno[1], S. Danielson[2], D. Kachel[1], N. B. Kachel[1,3], C. W. Mordy[1,3],

[1]NOAA Pacific Marine Environmental Laboratory
7600 Sand Point Way NE
Seattle WA 98115-0070
Phone: (206) 526-6453
Fax: (206) 526-6485
Phyllis.stabeno@noaa.gov

[2] University of Alaska, Fairbanks,
Fairbanks AK

[3] University of Washington/JISAO,
Seattle, WA 98105

For submission to Bering Sea Special Issue 4
Deep Sea Research II

January 8, 2016

Abstract

More than 20 years of data from moorings, satellite-tracked drifters and hydrographic surveys are integrated to provide a comprehensive view of currents and transport on the eastern Bering Sea shelf. The major sources of water onto the eastern Bering Sea shelf are North Pacific water flowing through Unimak Pass and Bering Slope water flowing onto the shelf usually via the canyons that intersect the shelf break. Absolute geostrophic transport through Unimak Pass varies from an average of 0.25×10^6 m^3 s^{-1} (Sv) in the warm months to 0.43 Sv in the cold months. Flow along the 50-m isobath is weak, with a transport of < 0.1 Sv (calculated from current meters) in summer and fall. The transport along the 100-m isobath measured at two locations is more than twice that along 50-m isobaths; in the summer at the Pribilof Islands it was 0.2 Sv and during spring and summer at 60°N the northward geostrophic transport (referenced to the bottom) was 0.31 Sv. Northward transport along the 100-m and 50-m isobaths accounts for approximately half of the transport through Bering Strait. A typical transit time from Unimak Pass to Bering Strait is >13 months and from Amukta Pass to Bering Strait via the Bering Slope Current is >8 months. Consequently, the source of most of the heat transported into the Arctic through Bering Strait is a result of air-sea interactions local to the northern Bering Sea. Analysis of the currents and water properties on the southern shelf indicates that ~50% of the shelf water is exchanged with slope water during October–January each year. This elevates the October mid-shelf average nitrate level from 6 μM to 14-16 μM by the end of January.

Keywords: Bering Sea, currents, transport, onshelf transport, nutrient replenishment

1. Introduction

The Bering Sea stretches > 1200 km from Bering Strait to the Alaska Peninsula, and 500 km from the coast of Alaska to the continental shelf break. While the shelf break is cut by a number of large canyons, including Bering Canyon in the south and Pribilof and Zhemchug Canyons farther north (Fig. 1), the eastern Bering Sea shelf itself is relatively flat (typical slope of 4×10^{-4}) with a maximum depth of 180 m at the shelf break.

The large horizontal spatial scales, and low bathymetric relief contribute to the relatively weak (< 5 cm s^{-1}) mean currents over much of the shelf (e.g., Kinder and Schumacher, 1981; Coachman, 1986). Exceptions to the weak flow on the southern shelf include flow along the 50-m and 100-m isobath (Schumacher and Stabeno, 1998; Reed, 1998) and anti-cyclonic tidally rectified circulation around the Pribilof Islands (Kowalik and Stabeno, 1999; Stabeno et al., 2008). North of ~60°N, flow intensifies along the east coast of Siberia forming the Anadyr Current (Kinder et al., 1986), and in the approach to Bering Strait, where the large (0.8 Sv (1 Sv = 10^6 m^3 s^{-1}) volume flux into the Arctic (Woodgate and Aagaard, 2005) is constricted by coastlines.

Much of the background flow field on the northern Bering shelf is set by the net Pacific-Arctic pressure head (Stigebrandt, 1984; Aagaard et al., 2006), which determines the mean northward flow through Bering Strait and the location of the western-intensified Anadyr Current (Kinder et al., 1986). Wind stress drives the dominant portion of the synoptic-scale (35-100 hr) variability in the coastal domain and north of 62° N (Danielson et al., 2012a, 2014).

The wind's influence manifests itself through both direct and remote forcing - surface Ekman transport drives coastal convergences and divergences that can trigger continental shelf waves, which rapidly propagate away from the generation region (Danielson et al., 2014). In addition to the magnitude of the wind stress, the relative orientation of the wind with respect to the orientation of the shelf break and coastline is critical for determining the response of the shelf currents to wind forcing (Danielson et al., 2012a, 2012b). Together, these determine how the synoptic wind-forced flows modify the mean flow field.

Aagaard et al. (2006) estimated that the source of approximately half of the flow on the Bering Sea shelf is the Gulf of Alaska's (GOA) Alaska Coastal Current (ACC). The ACC originates at the head of the GOA and flows southwestward along the southern coast of the Alaska Peninsula. Average ACC transport in the northern GOA is ~1 Sv of which ~30% enters the Bering Sea through Unimak Pass, providing relatively warm, fresh and nutrient-poor water to the southeastern Bering Sea shelf (Stabeno et al., 2002, in press; Aagaard, et al., 2006). This water mixes with slope water from Bering Canyon and then most of it eventually flows northward along either the 50-m or 100-m isobath (Reed, 1998; Stabeno et al., 2002). While flows concentrated along the 50-m and 100-m isobaths have long been known (e.g., Kinder and Schumacher, 1981; Coachman, 1986), measurements providing estimates of the magnitude of transport have been limited and the continuity of these flows has not been examined.

This paper uses extensive data sets from moorings, satellite-tracked drifters and hydrographic transects collected over a 20+ year period to examine currents on the eastern Bering Sea shelf. The goal is to spatially integrate our knowledge of flow on the shelf including transport along the 50-m and 100-m isobaths, transit times and the organization of the weak flow over the middle shelf. Using a map of currents derived using >400 trajectories from satellite-tracked drifters, estimates of how long it takes a parcel of water to transit from Aleutian Islands to Bering Strait are made. Transports through Unimak Pass, and along the 50-m and 100-m isobaths (two of the primary currents on the Southeastern Bering Sea shelf) are then derived. The organization of the weak flows on the middle domain is then examined. Utilizing the ~20 years of data collected at M2, estimates of nutrient replenishment on the southern shelf are calculated. Section 4 provides a summary of the results and conclusions.

2. Data and methods

2.1 Sea ice

Two sources of sea-ice data were used. The first source was the National Ice Center (NIC; http://www.natice.noaa.gov/), with data available from 1972 to 2005; the second source was the Advanced Microwave Scanning Radiometer EOS (AMSR; http://nsidc.org/data/amsre/) with data available from 2002 to 2014. These two data sets cover the entire period in which high quality data of sea-ice extent and areal concentration are available.

NIC data from 1972 to 1994 are from their publically available CD of data on a 0.25° grid. Later data (1995-2005) were downloaded from their website and interpolated it to the same positions. NIC data are derived from a variety of sources, including the Advanced Very High Resolution Radiometer (AVHRR) aboard the Polar Orbiting Environmental Satellites (POES). AMSR data consist of daily ice concentration data at 12.5 km resolution, which are available from the National Snow and Ice Data Center (NSIDC) website.

2.2 Reanalysis winds

The National Center for Environmental Prediction (NCEP) – Department of Energy Reanalysis uses a state-of-the-art analysis/forecast system to perform data assimilation on a 2.5° latitude by 2.5° longitude grid with data ranging from January 1979 to August 2012 (Kalnay et al., 1996; Kanamitsu et al., 2002). Six-hourly wind and wind stress data were extracted from the NCEP Reanalysis and interpolated to the desired mooring locations. NCEP Reanalysis data were obtained from the NOAA Earth System Research Laboratory, Physical Sciences Division in Boulder, Colorado, USA, from their website at http://www.esrl.noaa.gov/psd/. NCEP winds are well correlated with the observed winds in the Bering Sea (Ladd and Bond, 2002).

2.3 Moored hydrography and currents

Moorings (Table 1) have been deployed at many sites on the Bering Sea shelf, including surface and subsurface moorings instrumented with point current meters (Aanderaa recording current meters—RCM4 prior to 1998, RCM7 from 1995 to 2005, and RCM9 since 1996) and subsurface moorings containing acoustic Doppler current profilers (ADCP; Teledyne RD Instruments). Also, each of the moorings usually contained instruments measuring temperature and salinity at multiple depths. The ADCPs were upward looking, bottom-mounted, and either 300 or 600 kHz.

Data were collected at least hourly and all instruments were calibrated prior to deployment. The data were processed according to manufacturers' specifications. All current meter, temperature and salinity time series were low-pass filtered with a 35-hr, cosine-squared, tapered Lanczos filter to remove tidal and higher-frequency variability, and re-sampled at 6-hour intervals.

2.4 Shipboard hydrography

Conductivity-temperature-depth (CTD) measurements were made using a Sea-Bird SBE 911plus system with dual temperature and salinity sensors. Data were recorded during the downcast, with a descent rate of 15 m min^{-1} to a depth of 35 m, and 30 m min^{-1} below that. Salinity calibration samples were taken on at approximately half of the casts and analyzed on a laboratory salinometer.

*2.5 Satellite-tracked drifter*s

Since 1986, over 500 satellite-tracked drifters (drogue centered at ~40 m) have been deployed in the North Pacific and Bering Sea by investigators from the EcoFOCI program at Pacific Marine Environmental Laboratory (www.ecofoci.noaa.gov/drifters/efoci_driftersIntro.shtml). During 1986-1988, “holey sock” drogues were used, between 1987 and 1993 “tristar” drogues were employed, and from 1994 onwards “holey sock” drogues were again used. At these high latitudes, an average of ~14 position fixes per day were obtained from Argos. Spurious data were deleted from the time series, and data collected after the drogue was lost, or the drifter went aground or entered into ice (determined from maps of ice extent) were also deleted. The resulting time series were then linearly interpolated to hourly intervals.

Lagrangian velocities were determined by centered differences using the hourly drifter positions. A low-pass filter (25-hour running mean) was applied to the drifter location data. The methods used in deriving gridded mean velocities are described by Stabeno and Reed (1994), with each 2-day period within a grid area considered an independent estimate. The size of each grid cell was 0.5° latitude by 1° longitude. If the derived scalar speed did not exceed one standard error, or if there were 8 or fewer independent estimates within a grid cell, data were not used in the average vector plots, unless noted.

2.6 *Calculation of transport*

The hydrographic data were used to calculate baroclinic geostrophic transport (referenced to the bottom of the water column and hereafter referred to as simply geostrophic transport), and absolute geostrophic transport (the sum of the geostrophic transport and the bottom currents measured by the current meter). In contrast, total transport was calculated using currents measured at multiple depths on the moorings.

Estimates of total transport were obtained near Nunivak, St. Paul and St. George Islands, at Slime Bank and in Unimak Pass, following application of the approach previously applied to Shelikof Strait (Schumacher et al., 1989; Stabeno et al., 1995), Gore Point (Stabeno et al., 1995) and the Alaskan Stream (Stabeno and Hristova, 2014). In this approach the current data were low-pass filtered and the component of velocity normal to the mooring line was calculated. (When there was only one mooring, e.g., St. George Island, the net direction was used.) This normal component of velocity at each current meter or ADCP bin was multiplied by the cross-sectional areas defined by the midpoints located halfway between two adjoining moorings or total distance between the mooring and the shore, as appropriate. The outer edges of the mooring lines at Nunivak Island (IF array, Fig. 1), Slime Bank (SB) or St. Paul Island (PI), were defined as the same half distance as between the outer mooring and its nearest more coastal neighbor. The vertical boundaries were the surface, the bottom or the halfway point between instruments/bins as appropriate. The individual mooring transport time series were summed, providing a total transport perpendicular to each mooring line. The barotropic transport in Unimak Pass was calculated by multiplying the bottom currents normal to the pass by the cross sectional area of the pass.

3. Results and Discussion

3.1 Major current patterns

The major current patterns at a depth of 40 m are evident in the map of mean current velocities derived from satellite-tracked drifter trajectories (Fig. 2). The vectors represent currents when ice was not present in the grid cell. The ACC in the GOA is the weaker, southwestward flow evident on the shelf south of the Alaska Peninsula and Unimak Island, which enters the Bering Sea through Unimak Pass, while the Alaskan Stream is the stronger, southwestward flow along the slope, which enters the Bering Sea through the deeper Aleutian Passes, particularly Amukta Pass (171°W). The flow through Unimak Pass diverges into two branches: one follows the 50-m isobath and the other flows just seaward of the 100-m isobath. South of St. George Island the shelf narrows, forcing the flow to intensify before it turns northward. In the basin, the northward flow through Amukta Pass joins the northeastward flowing Aleutian North Slope Current (ANSC; Reed and Stabeno, 1999). Upon nearing Bering Canyon, the ANSC turns northwestward forming the Bering Slope Current (BSC). A portion of the BSC flows onto the shelf through the northern branch of Zhemchug Canyon, joining the100-m isobath flow northward. Near 63°N, the flow along the 100-m isobath joins with slope waters to form the Anadyr Current, which flows anti-cyclonically around the Gulf of Anadyr. Elsewhere on the shelf, average flows are weak.

Many of the satellite-tracked drifters presented here were deployed on the southern Bering Sea shelf in the spring and by the time they reached 60°N, autumn usually had already arrived. With the advent of winter and its stronger winds, the mixed layer deepened to below the drogue depth, so the drifters became more responsive to winds. More importantly, by the time many of the drifters approached St. Matthew Island, ice had begun to arrive (Stabeno et al., 2012a), thus ending the drifter record. This resulted in fewer and less reliable estimates of velocity on the northern shelf than farther south.

While drifter trajectories provide an indication of flow patterns and velocities at 40 m, they do not provide information on the magnitude of the transport. In the following three sections, we will discuss the magnitude of transport through Unimak Pass and along the 50-m and 100-m isobaths.

3.2 Inflow through Unimak Pass

Barotropic transport (estimated from near-bottom current measurements) through Unimak Pass varied seasonally, with the greatest transport in fall to mid-spring and the weakest from May to September (Fig. 3a). Transports were positively correlated ($r = 0.7$; Stabeno et al., 2002) with the southwestward winds (defined as the direction the winds are moving to). Mean barotropic transport was calculated using current data from five Unimak Pass (UP) deployments (Table 1). During October 1–April 25 transport was 0.25 ± 0.03 Sv (mean ± standard error of the mean) and during May 10 – September 15 it was 0.08 ± 0.02 Sv, or approximately three times larger in the winter than summer.

Variability in the geostrophic transports through Unimak Pass (Table 2) was calculated using four standard hydrographic stations. Stabeno et al. (2002) noted that the transport was three times as large during ebb tide as during slack tide. Based on 32 hydrographic transects, a comparison of winter and summer transports can be made. The geostrophic transports in the cold months (October 1–May 14) and warm months (May 15–September 30) were approximately the same: 0.16 ± 0.17 Sv (mean ± std) in the warm season and 0.18 ± 0.10 Sv in the cold season. Historically, estimates of absolute geostrophic transport have been calculated by combining a barotropic component calculated using near-bottom currents and the geostrophic component referenced to the bottom from hydrographic surveys (e.g., Fandry and Pillsbury, 1979; Reid 1986; Stabeno et al., 2002). The absolute geostrophic transport through Unimak Pass was ~0.25 Sv in the warm months and ~0.43 Sv in the cold months. This difference was primarily driven by the barotropic component, which differs significantly between summer and winter.

In 2002, an ADCP was deployed in the narrow passage to the south of Unimak Pass. The currents measured throughout the water column yielded time series of total transport (Fig. 3b, black line) and the bottom current bin was used to calculate the barotropic transports (red line). The records are clearly well correlated. During this two and half month period, the mean barotropic transport was ~0.10 Sv, while the mean total transport was ~0.22 Sv, a difference of 0.12 Sv. This difference is similar to the mean geostrophic transport calculated from hydrographic data (Table 2).

There are no estimates of the magnitude of flow in Bering Canyon based on direct observations, but trajectories of satellite-tracked drifters show onshelf advection associated with this canyon (e.g., the purple trajectory in Fig. 4). The flow up Bering Canyon may combine with the transport through Unimak Pass, resulting in greater transport onto the southeastern shelf than that solely from Unimak Pass. Trajectories in Figure 4 also suggest a separation into flow along the 50-m and the 100-m isobaths.

3.3 Flow along and near the 50-m isobath

Only a few moorings have collected time series of currents, temperature and salinity along or near the 50-m isobath north of Unimak Island and the along the Alaska Peninsula. Many of the earlier observations were based on short (< 3 month) measurement intervals (e.g., Kinder and Schumacher, 1981). In the next section, we examine data from longer deployments, near Unimak Island and farther north near Nunivak Island.

3.3.1 Mean currents and transport along the 50-m isobath

Following the 50-m isobaths northeastward from Unimak Pass, moorings were deployed in 1995, 1997, 1998 and 1999 (Table 1; Fig. 1). The southernmost moorings were deployed from February to September 1995 (Table 1) at M1 in 67 m of water. They revealed northeastward flow parallel to the peninsula (Fig. 5). The flow at 15 m (net flow 3.5 cm s^{-1} at 65°) was much stronger than at 63 m (net flow 0.6 cm s^{-1} at 73°). In the summer of 1999, another set of moorings (SB1, SB2, and SB3) was deployed to the east of Unimak Pass and M1 between water depths of 38 m and 97 m (Fig. 1). Current meter data from these moorings were used to calculate a time series of total transport (Fig. 6), which ranged from -0.25 Sv to 0.35 Sv, with an average of 0.04 Sv.

The salinities can be used to give an indication of the sources of the flow near M1 and the SB line. Unfortunately, the conductivity sensors on the SB moorings suffered from heavy biological fouling in this region, which is appropriately referred to as "Slime Bank." An examination of tidal variation from salinity time series collected in 1995 (not shown) reveals that the variation in salinity at tidal frequencies was ~0.2, with increasing salinity during flow onto the shelf. While the salinity time series from 1995 were short, the low-pass filtered salinity varied by ~0.4, with more saline water associated with northeastward flow. The water was more saline in the 1999 time series than in 1995 (likely because the salinity in 1999 was measured at 84 m, ~ 40 m deeper than that in 1995), but with a similar pattern of increasing salinity in May. The salinity of the water that flows through Unimak Pass varies seasonally (Stabeno et al., 2002), with the lowest salinity (< 31.6) occurring in January and highest (>32) in late summer. The higher salinities observed in 1999, indicate that the source of this water was likely Bering Canyon, or a combination of waters from Bering Canyon and Unimak Pass.

The only other site with multiple moorings across the 50-m isobath was the Inner Front (IF) cluster near Nunivak Island. Time series of total along-shelf transport derived from current measurements at these moorings showed strong variability (Fig. 7), but the correlation between transport and winds was not significant at the 99% level. Mean transport in the summer of 1997 and 1998 was ~0.05 Sv toward the northwest, with stronger transport (~0.1 Sv) in the fall of 1997.

Danielson et al. (2012a) examined currents from eight year-long moorings deployed on the 55 m, 40 m, and 25 m isobaths in July 2008 and again in July 2009. Six of these moorings were deployed north of the IF moorings on the central (C) line and northern (N) line (Fig. 8a). The two deployed on the southern (S) line were within the same area as the IF cluster. At the S and the IF mooring sites, mean currents were parallel to bathymetry and the horizontal gradients of density, except at the shallower S mooring. Farther north, the net speed at the moorings on the N line was weak (< 2 cm s^{-1}), while flow on the C line was somewhat stronger, with currents at 5 and 10 m directed westward and southward, and deeper currents more northerly. Because of the large wind-driven subtidal variance, the mean currents were not statistically different than zero (at the 95% confidence level) except at 55 m on the C and S lines where 3-4 month seasonal means were as large as 3-4 cm s^{-1} in summer and fall.

The subtidal variability in flow on the N and C lines were largely forced by the winds (see Figure 17 in Danielson et al., 2012a), with northward winds generally forcing northward flow, and with southward winds resulting in weaker northward or even southward flow. This was also true for the inner mooring (at a depth of 40 m) on the S line. The flow at the deeper (55 m) mooring on the S line, however, was more complex. Subtidal variability in flow at 5 and 10 m was largely forced by winds, but the flow at 20 and 30 m was mainly northwestward and less affected by winds. This northwestward flow at the IF and the S moorings (Fig. 8 a, b) was associated with horizontal density gradients that characterize the inner front (Kachel et al., 2002). Interestingly, during winter this density gradient can reverse sign as a result of extensive brine production in shallow waters (Danielson et al., 2012a), reversing the flow.

3.3.2 Correlations of currents along the 50-m isobath

Concurrent measurements of near-surface currents at M2 and three sites (SB2, CN, and IF2) along the 50-m isobath were made in 1999 (Fig. 1 and Table 1). CN, deployed at Cape Newenham, was ~280 km to the northeast of SB2 and ~ 300 km to the southeast of IF2. Correlations of these currents with NCEP Reanalysis winds ranged from 0.32 at CN to 0.69 at M2 (at a depth of 7 m), with a 95% significance level, ρ, of ~0.12. Correlations among moorings were weaker, with highest correlations occurring at 0 lag between M2 and CN (r=0.41, ρ = 0.12). Near surface currents at IF2 lagged both M2 and CN by 6 hrs (r=0.35, ρ = 0.12) and 12 hrs (r=0.28, ρ = 0.13), respectively. Currents at SB2 also lagged the surface currents at M2 (r= 0.26, ρ = 0.13) and CN (r= 0.26, ρ = 0.13), but by larger amounts (18 hr and 24 hr, respectively).

Together, the above analyses suggest a relatively heterogeneous flow field on the 100-300 km scale of the mooring separations. Reasons for local differences may be driven by variations in the atmospheric forcing over these length scales and differences in the timing of these forcings, unresolved three-dimensional aspects of the flow field, and the influences of the varying orientation of coastlines and seafloor topography. While the data set is not ideal, this analysis provides no evidence of propagating coastal trapped waves in this region.

3.4 Transport along the 100-m isobath

Having discussed the 50-m flow, we will return to Unimak Pass and examine the 100-m flow. There are two locations along the 100-m isobath where moorings have been deployed and the necessary data were collected to calculate total transport. The first set of locations (SG2 and SG3) is on the narrow (< 30 km) shelf, which extends southward from the southern tip of St. George Island to the shelf break (Fig. 1). The second set (PI3 and PI5) is farther north on a line extending westward from the western tip of St. Paul Island.

3.4.1 Transport south of St. George Island and west of St. Paul Island

Three times during the interval 1997–1999, moorings were deployed south of St. George Island for 5-6 months. In 1997 a mooring was deployed on the 200-m isobath (SG2), while in the springs of 1998 and 1999 moorings were deployed on 100-m isobath (SG1). On this narrow shelf, an estimate of transport was made for spring and summer of 1998 and 1999 using velocity data from SG1 (Fig. 9a). Mean transports were similar in the two years: 0.20 Sv in 1998 and 0.18 Sv in 1999. In both years the flow was generally westward with considerable variability, including periods of reversal on time scales of 3-5 days. These reversals are likely associated with periods of northward flow that occur occasionally east of St. George Island (Stabeno et al., 2008). The flow along the 100-m isobath west of St. Paul Island also showed considerable temporal variability (Fig. 9b), but with fewer and weaker reversals. The mean total transport east of St. Paul Island was 0.25 Sv. The magnitude of these summer transports near the 100-m isobath is similar to that through Unimak Pass.

The lack of current measurements along the 100-m isobath near the Pribilof Islands in winter prevents quantitative winter comparisons between transports at the Pribilof Islands and through Unimak Pass. Some more qualitative comparisons, however, can be made. First, the mean and standard deviation of the current velocity in the upper 100 m at SG2 during June–September 1997 was 7.1± 5.5 cm s^{-1} westward, which was similar to the 7.0 ± 6.7 (6.0 ± 9.7) cm s^{-1} measured in 1998 (1999) at SG1. While SG2 was at the edge of the shelf, trajectories (not shown) of the satellite-tracked drifters (drogued at 40 m) indicated that the flow along the 100 m and at 200 m isobaths was uniform. Thus, the flow at SG2 is probably representative of the flow at SG1. Moored current observations at SG2 during the winter show that winter currents were almost 50% stronger than the summer currents (see Fig. 7 in Stabeno et al., 2008). Thus, it is likely that winter currents at SG1 would also be stronger than those in the summer. Second, mean Lagrangian velocity in the 50 km × 100 km box (166–167°W, 55.4–56.4°N) south of St. George was marginally stronger in October–April (4.5 cm s^{-1} ± 0.4 cm s^{-1}, mean ± standard error) than in May–September (3.7 ± 0.5 cm s^{-1}). In contrast to these two observations, data from the long-term mooring at 135 m depth (M3; not shown) exhibited no seasonal variability in the current. The observed seasonality in flow at Unimak Pass and near the Pribilof Islands compared with the lack of seasonality in between these sites suggest the presence of cross-isobath exchanges in the region (Cokelet, 2016).

3.4.2 Transport north of 58°N along the 100-m isobath

That flow continues northward along the 100-m isobath is evident in the satellite-tracked drifter trajectories (Fig. 10) and in the vectors derived from those trajectories (Fig. 2). Individual drifter trajectories show northward flow seaward of the 100-m isobath as far north as St. Matthew Island (Fig. 10a). In addition, some drifters that were caught in the BSC show onshelf flow in Zhemchug Canyon. These drifters were also advected northward over the shelf, usually remaining west of the drifters that were traveling along the 100-m isobath (Fig. 10b). The monthly average velocity of the drifters typically ranged from 5 to 10 cm s^{-1}, unless caught in an eddy (e.g., red in Fig. 10a).

Lacking moorings along the 100-m isobath north of the Pribilof Islands, estimates of transport depend on hydrographic transects. Since 2005, the east-west line just south of St. Matthew Island (MN line, Fig. 1) has been occupied a dozen times (Table 3), revealing a mean geostrophic transport of 0.31 ± 0.05 Sv. There were strong cross-shelf gradients in nutrients, temperature and salt along the MN line, with more saline, nutrient-rich water offshore and at the bottom of the water column (Fig. 11 a,b). Geostrophic currents, referenced to the bottom, indicate higher speeds (~5 cm s^{-1}) along the 120-m isobath seaward of the two-layer structure of the middle domain and a weaker relative maximum (>2 cm s^{-1}) just shoreward of the 100-m isobaths (Fig. 11c). Arguably, the 120-m flow is from the northern lobe of Zhemchug Canyon and 100-m flow is the continuation of the 100-m isobath flow near the St. Paul Island.

3.5 Time scales of northward flow along the 100-m isobaths and in the BSC

The map of velocity vectors (Fig. 2) provides the opportunity to estimate how long it would take a drifter (or parcel of water) to travel from the southern boundary of the eastern Bering Sea north to Bering Strait. Two continuous pathways can be examined (Fig. 12): the first is flow through Unimak Pass and along the 100-m isobath, and the second is through Amukta Pass following the ANSC/BSC to Zhemchug Canyon and onto the shelf there. A third pathway that follows the BSC to the northern boundary of the basin cannot be investigated because the current vectors in Figure 2 do not show the flow coming onto the shelf at the northern edge of the basin.

A drifter originating in Unimak Pass would take ~4 months to pass St. George Island and 13 months to reach the vicinity of St. Lawrence Island (Fig. 12a), if there was no ice. Using the monthly average maps of ice concentration derived from the AMSR data set (not shown), a drifter exiting Unimak Pass in October would come in contact with ice just north of St. Paul Island, while a drifter exiting Unimak Pass in November would follow the ice as it retreats northward and only come into contact with sea ice the following November near St. Lawrence Island. In contrast, a drifter being advected northward by the BSC would reach the area to the west of St. Matthew Island in six months (Fig. 12b), three months faster than the shelf route. So, in an average year, drifters exiting Amukta Pass in the four months from October to January would reach Bering Strait 9-10 months later before encountering ice. These water parcels, however, would be subjected to cooling over the southern Bering Sea by air-sea interactions during fall and winter.

The duration of the trip north has implications for heat from the GOA entering the Chukchi Sea. On the transit north, any parcel will be influenced by air-sea-ice interactions. Ice plays a particularly profound role if the bottom depth is less than ~120 m, in that it can cool the entire water column to the freezing point (Stabeno et al., 2001). Any parcel of water following the 100-m isobath would come into contact with sea ice, prior to reaching the Arctic, effectively removing the GOA heat signature. Thus, the source of heat reaching the Arctic *via* the 100-m isobath is from air-sea interactions in the Bering Sea (Wood et al., 2015). Some heat from the GOA could reach the Arctic following the BSC route, but during the ~8 months of transit, local air-sea interaction would also modify the water. Other waters bound for Bering Strait could include BSC waters not originating in Amukta Pass but these waters too will have spent the greater part of a year (at a minimum) in the Bering Sea. The implication is that most of the heat entering Chukchi Sea through Bering Strait originates from air-sea fluxes in the northern Bering Sea.

3.6 Organized flow on the middle shelf

In contrast to the flow along the 50-m and 100-m isobaths, the flow on the middle shelf has been viewed as weak, with an implication that there is no consistently organized pattern on this part of the shelf. Long-term observations at four primary mooring sites (M2, M4, M5, and M8; Fig. 1, Table 1) are revising this view (Stabeno et al., 2010, 2012a).

3.6.1 Monthly and long-term mean currents at M2, M4, M5 and M8

Examination of the monthly mean flow at each of the sites showed marked similarity in direction and magnitude of the flow at M2 and M4 (Fig. 13 c,d), with stronger flow in September through March and weaker flow during summer. The annual mean (1995-2013) flow at M2 was westward, with weak (0.2 cm s^{-1}) near-bottom currents (~60 m in 72 m of water) and stronger (1.5 cm s^{-1}) near surface (~15 m) currents. In the near surface, the annual mean flow at M4 was toward the south-southwest and weaker (1.0 cm s^{-1}) than at M2. The near-bottom current was toward the southwest and identical in magnitude (0.2 cm s^{-1}) to that measured at M2.

In contrast to the currents at M2 and M4, the monthly mean flows were stronger at M5, with predominantly northwestward flow in January through April (Fig. 13b). The flow weakened during the summer and then strengthened and turned southwestward in November. The long-term mean currents were stronger at M5, especially in the fall and winter, than at M2 or M4, with average westward flow of 2.0 cm s^{-1} in the upper water column and 0.6 cm s^{-1} toward the southeast in the near bottom (~60 m in 73 m of water).

Finally, monthly average currents at M8 were weak (mostly < 1 cm s^{-1}) from January through August, with the strongest currents in late summer and fall (Fig. 13a). Average near-surface (~15 m depth) flow using ~8 years of data was northwestward at 0.8 cm s^{-1}, and the near-bottom flow was northwestward at 0.4 cm s^{-1}.

3.6.2 Mooring sites M2 and M4: Differences between warm and cold years

The long time series at M2 (>18 yrs) and M4 (>14 yrs) allow comparison of currents in the “warm” years and in the “cold” years. Stabeno et al. (2012b) identifies 1995, 1997, 1999, and 2007-2010 as cold, 1998 and 2001–2005 as warm, and 1996, 2000, and 2006 as average. Recent temperature data from M2 categorized 2011 as average and 2012–2013 as cold. It should be noted that the time series at M5 and M8 are not long enough to divide into warm/cold years and that, in addition, the definition of warm and cold years from Stabeno et al. (2012b) only applies to the southern shelf. Warm and cold years in the north do not align with warm and cold years in the south (Stabeno et al., 2012b; Danielson et al., 2011; Luchin and Panteleev, 2014).

A strong seasonal signal is evident in the time series, along with significant differences in near-surface current direction and/or magnitude between warm and cold years in December–June (Fig. 14). The currents were stronger in cold years at both M2 and M4 and the flow during the winter months was directed more southward than during warm years. This depiction is consistent with the flow field responding to changes in the wind stress over the Bering shelf causing west-east displacement of the Aleutian Low as described by Danielson et al. (2011, 2012a, 2012b, 2014). In particular, years with storms located over the GOA are generally associated with cold years and greater southward (or less northward) advection near M2 and M4. Near-bottom currents were weaker, with the greatest differences between warm and cold years occurring between December and February.

Factors that can cause differences in currents between warm and cold years include winds, the presence/absence of ice, and the horizontal density structure. Data exist to examine the first two mechanisms (see following section), but there is a paucity of hydrographic transects within the sea ice and around the melting ice edge. This is especially true in December–February when the flow differences between warm and cold years are greatest and magnitude of flow is the strongest.

3.6.3 Mooring sites M2 and M4: Effect of winds and ice on currents

While the correlation between winds and currents at 5–10 m were substantial (e.g., 1999, r = 0.7), the correlations between winds and currents at ~15 m were generally weaker (r < 0.3). For example, the maximum vector correlation between M2 near-surface (~15 m) current and NCEP Reanalysis winds in 2007–2008 was 0.27 at a lag of 12 hours and rotation of 91°. While the correlation was significant (ρ =0.10), the wind directly explained only 7% of the current variance.

To further examine the impact of winds and ice on the currents, the year was divided into three periods: “summer” (May 15–September 15); winter no-ice (October 15 until arrival of ice at areal concentrations > 30%); and winter with ice (when ice is present at > 30% areal concentrations and before March 31). If ice was present after May 15, the data were not included in the “winter” or the “summer” estimates. In each of these periods, winds (> 4 m s^{-1}) were binned by direction into octants (0-45°, 45-90°, etc.). The currents, lagged by 18 hours, associated with those wind directions were then averaged.

During the winter period with no ice, surface current directions at M2 were dominantly along the southwest–northeastward axis with none of the average currents directed toward the two southeastern octants (Fig. 15a). In some months, mean near-bottom currents, representing the barotropic component of the flow, opposed the direction of the winds (Fig. 15b). When the averaged near-bottom currents were subtracted from near-surface currents, the resultant velocities (Fig. 15c) were found to be largely wind-driven (45°-90° to the right of the wind), but flows to the southwest were still stronger. Figures 15a and 15b provide some insight to the three-dimensional nature of the flow field by depicting the direction in which the near-surface and near-bottom currents are oriented relative to each other. The presence of both surface and near-bottom Ekman layers, in addition to the varying influences of stratification, fronts, and topographic constraints all confound interpretation of the near-bottom currents on this shallow shelf.

During periods when areal ice cover exceeded 30% (not shown), the surface currents at both M2 and M4 were largely westward, forced by the southward and southwestward winds. Momentum is transferred from the winds to water directly (if not 100% ice cover) and via the ice motion. During summer the near-bottom currents at M2 and M4 were weak (<1 cm s^{-1}) and the near-surface currents were wind driven.

3.6.4 Mooring site M5

Of the four mooring sites on the middle shelf, the highest correlations between the currents and the winds occurred at M5. Maximum vector correlations between the winds and the near-surface currents were 0.45 at an angle of 71° with the currents lagging by 12 hr. The 95% significance level was 0.1. Correlations between winds and near-bottom currents were weaker, but still significant.

The position of M5 is unique among the four middle-shelf mooring sites. Unlike M2 and M4, which are distant from land, it is within 50 km of the inner front and just south of St. Matthew Island. A polynya often forms southwest of St. Matthew Island (Stringer and Groves, 1991), and early winter peaks in salinity in 2005-2008 (Fig. 16) could be related to the increase in salinity resulting from ice formation (brine rejection). The lower salinities in 2010 and much of 2013 were likely associated with westward flow, and the advection of fresher coastal domain water to the site as discussed by Danielson et al. (2011, 2012b). Trapping of waters near St. Matthew Island through tidal rectification (e.g., Kowalik and Stabeno, 1999) may also retain melt waters in this vicinity.

The stronger flow, the proximity to the inner front and to St. Matthew Island, and its position in the transition zone between the northern shelf and the southern shelf (Stabeno et al., 2012a) place M5 in a region of greater environmental variability than the other mooring sites. West of M5, the northward flow along the 100-m isobath (Fig. 10) introduces nutrient-rich bottom water to latitude of M5 (Fig. 11b), so eastward flow can then introduce higher concentrations of nutrients and salt to the region around M5 (Mordy et al., 2010). Finally, sea ice plays an important role here. Brine formation from the polynya at St. Matthew Island can introduce higher salinity water into the region around M5. In contrast, ice melt reduces the surface salinity both on its arrival in late fall/early winter and its retreat in spring (Sullivan et al., 2014). As a consequence, the salinity at M5 is highly variable.

3.6.5 Mooring site M8

The currents at M8 were only weakly correlated with local winds ($r = 0.31$ for near-surface flow and $r = 0.25$ for near-bottom flow). The 95% significance level for both was 0.1. The cause of the weak correlation is not completely clear, although it may be influenced by the large-scale pressure gradient that drives flow through Anadyr Strait, the proximity of M8 to the orographically influenced tip jets that develop in the Gulf of Anadyr (Moore and Pickart, 2012), or the limitations of the relative coarse NCEP reanalysis model. Aspects of the role of remote winds are discussed in Danielson et al.

(2014), including the potential for shelf winds both north and south of Bering Strait to trigger short-lived but energetic continental shelf waves.

From January through August, the monthly mean flow at M8 was relatively weak and highly variable (Fig. 13a). The surface flow during the remaining four months of the year was stronger and more organized toward the west or northwest (Fig. 17). This westward flow advected colder water over the mooring before the arrival of ice. By the time ice arrived, usually in December, the water was already near the freezing point (Sullivan et al., 2014). This resulted in minimal ice melt and minimal freshening of the water at this location during fall, although during the spring, melting ice decreased the surface salinity by ~0.5.

In contrast to the highly variable conditions near M5 and conditions near M2 and M4, the regime at M8 is more strongly influenced by extensive annual sea-ice cover. In addition, the weak flow in the summer coupled with the weak tides has implications for the bottom water chemistry. The local export of primary production to the seafloor near M8 results in a thriving benthic community (Grebmeier, et al., 1988) where respiration products (CO_2) can accumulate over time. The weak currents do not flush this water, and so the combination of respiration and anthropogenic CO_2 results in pH levels low enough to dissolve both aragonite and the much harder calcite (Cross et al., 2013).

3.7 Replenishment of salt and nutrients on the shelf

The flow up Bering Canyon and the flow through Unimak Pass likely play a role in replenishing salt (lost due to advection of ice and subsequent melting during winter and spring, Sullivan et al., 2014) and nutrients (consumed by phytoplankton blooms in spring and summer) on the southeastern Bering Sea shelf. During summer, the frontal structure of the inner front and middle transition isolates the water on middle domain (Coachman, 1986), but with the breakdown of the fronts in fall, cross-shelf fluxes increase (Danielson et al., 2011). At M2, the annual signal in salinity shows an increase (strong at the surface and weaker near the bottom) from October into January (Fig. 18a). The slight freshening of the near-surface layer in mid-January, likely resulted from the early arrival of ice in some years (e.g., 1997, 1998, 2013) and its subsequent melting (Sullivan et al., 2014). An estimate of the salt flux onto the shelf can be made by examining each year individually from the time the water column becomes well mixed (usually in October) until February or the arrival of ice (areal concentration > 20%), whichever is earlier. There are limited salinity observations in October–January from Bering Canyon or Unimak Pass, which are the sources of the more saline water. Ignoring the time of year and the shallow (<5 m deep) freshwater lens, which can occur in the vicinity of Unimak Pass, salinity varies from 31.4 to 32.8 in the upper 100 m, but more typically is near 32.35.

To calculate the percentage of water replenished each year on the shelf, four values of slope salinity (32.3, 32.35, 32.4, and 32.45) were chosen. Using these values, the percentage of water flushed at M2 is shown in Figure 18b. The year-to-year variability was not related to timing of ice arrival, nor to whether the previous year was warm or cold (defined in Stabeno et al., 2012b). Averaged over 1996-2012, the annual percentage of water flushed from the shelf between late October through January ranged from 48% (assuming a slope salinity of 32.45) to 62% (slope salinity of 32.3), suggesting that a bit more than half the shelf water in the vicinity of M2 is replaced in fall and early winter.

A reasonable value of depth-averaged fall nitrate concentration near M2 is ~6 μM (e.g., Stabeno et al., 2002, 2010; Mordy et al., 2012). The source of water along the slope is largely from Amukta Pass (Stabeno et al., 2005, 2009; Ladd, 2014) giving a fall/winter nitrate concentration at the slope of 25 μM (Mordy et al., 2005), while the average nitrate in Unimak Pass in February 1998 was 18 μM (Stabeno et al., 2002). Using a slope nitrate concentration of 22 μM and a shelf concentration in autumn of 6 μM, a 50% (60%) flushing of the shelf would result in a nitrate concentration of 14 (16) μM, or a nitrate replenishment of 57% (62%), which is similar to the 50% estimated by Whitledge et al. (1986) and in the upper range suggested by Granger et al. (2013).

4. Summary and Conclusion

Well defined, albeit weak, subtidal currents exist across much of the eastern Bering Sea shelf, with stronger flows along the 50 and 100-m isobaths and in the Anadyr Current. While varying in magnitude, these currents persist throughout the year. The time series of the annual velocity at M2 and M4 (~300 km apart) were similar, with strong mean westward flow in the late fall and winter and relatively weak currents during the summer. The near-surface currents were well correlated with reanalysis winds. Correlations decreased with increasing depth, but remained significant (95% level). The near-surface baroclinic flow (near-surface minus near-bottom), however, was well explained by Ekman dynamics and well correlated with the winds. At the northernmost mooring, M8, the flow was weak except in the fall, when westward flow cooled the water column, preconditioning it for the arrival of ice. At this site, the winds and currents were weakly correlated.

The source of much of the transport along the 50- and 100-m isobaths is Unimak Pass, where the transport ranges from a mean of ~0.2 Sv in the warm season to ~0.45 Sv in the cold season. Similar to the seasonal variations in Unimak Pass, flow past the Pribilof Islands varies between winter and summer with a similar phasing of the annual maxima and minima. Additional transport enters the shelf through canyons. Flow onto the shelf in Bering Canyon and from the Gulf of Alaska through Unimak Pass provides salt (including nutrients) to the southeastern shelf. From late October to February 1, approximately half the water is replenished in the vicinity of M2. This replenishment is an important source of nutrients for the following year's primary production, more than doubling the nitrate inventory that was present at the end of summer.

Northward geostrophic transport on the outer shelf at 60°N is ~0.34 Sv, accounting for over 40% of the total transport (0.8 Sv) through Bering Strait (Woodgate and Aagaard, 2005). The transport along the 50-m isobath (Bering ACC water) is appreciably smaller, ~0.05 Sv, and includes at least some water derived from the two largest Alaskan rivers entering the Bering Sea (the Yukon River [~6000 $m^3 s^{-1}$] and the Kuskokwim River [2000 $m^3 s^{-1}$]). The coastal ACC water is associated with the low-salinity plume of the Yukon River. The ACC contributes ~0.08 Sv to the transport through Bering Strait (Gawarkiewicz et al., 1994; Woodgate and Aagaard, 2005). The remaining fraction of the Bering Strait through-flow (~50%) likely arises from the Bering Sea slope as part of the Anadyr Current.

The average transit time on the Bering Sea shelf from Unimak Pass to Bering Strait along the 100-m isobath is 13-14 months. A second pathway originating at Amukta Pass is faster. This path follows the BSC to ~60°N where a portion of BSC flow crosses onto the shelf through Zhemchug Canyon, and eventually joins the flow along the 100 m isobath. Water traveling along this pathway (Amukta to Zhemchug to Bering Strait) can reach Bering Strait in 8 months. Thus, most of the heat entering into the Chukchi Sea through Bering Strait originates from air-sea interactions in the Bering Sea, not from the Gulf of Alaska.

The weak correlation between subsurface currents and winds on the middle shelf contrasts with the higher correlations between these variables in the coastal domain. In contrast, flow along the 50-m isobath is associated with the Inner Front (the boundary between the unstratified coastal and stratified middle domains), and flow along the 100-m isobaths is associated with middle transition (the boundary between the middle and outer domains). In these locations, the horizontal density structures contribute to the mean flows. Sea ice may further complicate the flow patterns, because of the creation of low salinity pools formed by melting ice and brine created through freezing. These features, however, are ephemeral.

Based on our analyses, a number of knowledge gaps exists limiting our understanding of the Bering Sea shelf circulation and its influence on bottom-up ecosystem controls. For example, the seasonality of currents in Unimak Pass and near the Pribilof Islands contrasts with the lack of seasonality midway between the two. These observations imply the existence of potentially important regional-scale cross-isobath exchanges. Drifter measurements are biased to ice-free locations and time intervals, leaving many aspects of the flow pathways in winter unexplored. Bering, Pribilof and Zhemchug Canyons all play an important role in introducing slope water onto the shelf, but there are few measurements addressing the magnitude and seasonality of flow in these canyons. Addressing these issues will improve our understanding of the time-varying nature of shelf-basin and Pacific-Arctic exchanges.

Acknowledgements

We thank S. Salo, W. Floering, and C. DeWitt for providing assistance at sea and were responsible for collecting the majority of our mooring data. K. Birchfield provided graphics work. We thank the officers and crews of the NOAA ships Miller Freeman and Oscar Dyson, R/V Thomas G. Thompson, and USCG Healy for invaluable assistance in making these oceanographic measurements. This research is contribution No. 4189 from NOAA/Pacific Marine Environmental Laboratory, #0862 to NOAA's Ecosystems Fisheries Oceanography Coordinated Investigations, contribution 582 from the North Pacific Research Board; and 179 from BEST/BSIERP. This publication is partially funded by Joint Institute for the Study of the Atmosphere and Ocean, University of Washington, contribution #2294. The research was generously supported by grants from the NSF-sponsored BEST (ARC-1108440, ARC-0732640 and ARC-0732430), the North Pacific Research Board (Grants: #517, 602, 701, 1302, and B52) and NOAA's North Pacific Climate Regimes and Ecosystem Productivity programs.

References

Aagaard, K., Weingartner, T.J., Danielson, S.L., Woodgate, R.A., Johnson, G.C., Whitledge, T.E., 2006. Some controls on flow and salinity in Bering Strait. Geophys. Res. Lett. 33, L19602, doi:10.1029/ 2006GL026612.

Coachman, L.K., 1986. Circulation, water masses, and fluxes on the southeastern Bering Sea shelf. Cont. Shelf Res. 5(1–2), 23–108.

Cokelet, E.D., 2015. 3-D water properties and geostrophic circulation on the eastern Bering Sea shelf. submitted to Deep Sea Research Part II: Topical Studies in Oceanography. This issue.

Cross, J.N., Mathis, J.T., Bates, N.R., Byrne, R.H., 2013. Conservative and non-conservative variations of total alkalinity on the southeastern Bering Sea shelf. Mar. Chem. 154, 100–112.

Danielson, S., Eisner, L., Weingartner, T., Aagaard, K., 2011. Thermal and haline variability over the central Bering Sea shelf: Seasonal and inter-annual perspectives. Cont. Shelf Res. 31(6), 539–554, doi:10.1016/j.csr.2010.12.010.

Danielson, S.L., Weingartner, T.J., Aagaard, K., Zhang, J., Woodgate, R.A., 2012a. Circulation on the central Bering Sea shelf, July 2008–July 2010. J. Geophys. Res. 117, C10003, doi:10.1029/2012JC008303.

Danielson, S., Hedstrom, K., Aagaard, K., Weingartner, T., Curchitser, E., 2012b. Wind-induced reorganization of the Bering shelf circulation. Geophys. Res. Lett. 39, L08601, doi:10.1029/2012GL051231.

Danielson, S.L., Weingartner, T.W., Hedstrom, K., Aagaard, K., Woodgate, R., Curchitser, E., Stabeno, P., 2014. Coupled wind-forced controls of the Bering–Chukchi shelf circulation and the Bering Strait through- flow: Ekman transport, continental shelf waves, and variations of the Pacific–Arctic sea surface height gradient. Prog. Oceanogr. 125, 40–61, doi:10.1016/j.pocean.2014.04.006.

Fandry, C., Pillsbury, R.D., 1979. On the estimation of absolute geostrophic volume transport applied to the Antarctic circumpolar current. J. Phys. Oceanogr. 9, 449–455.

Gawarkiewicz, G., Haney, J.C., Caruso, M.J., 1994. Summertime synoptic variability of frontal systems in the northern Bering Sea. J. Geophys. Res. 99, 7617–7625, doi:10.1029/94JC00259.

Granger, J., Prokopenko, M.G., Mordy, C.W., Sigman, D.M., 2013. The proportion of remineralized nitrate on the ice-covered eastern Bering Sea shelf evidenced from the oxygen isotope ratio of nitrate. Global Biogeochem. Cycles, 27(3), 962–971, doi: 10.1002/gbc.20075.

Grebmeier, J.M., McRoy, C.P., Feder, H.M., 1988. Pelagic-benthic coupling on the shelf of the northern Bering and Chukchi seas. I. Food supply source and benthic biomass. Mar. Ecol. Prog. Ser. 48, 57–67.

Kachel, N.B., Hunt, Jr., G.L., Salo, S.A., Schumacher, J.D., Stabeno, P.J., Whitledge, T.E., 2002. Characteristics and variability of the inner front of the southeastern Bering Sea. Deep-Sea Res. II 49, 5889–5909.

Kalnay, E., , Kanamitsu, M., Kistler, R. Collins, W., Deaven, D., Gandin, L., Iredell, M., Saha, S., White, G., Woollen, J., Zhu, Y., Leetmaa, A., and Reynolds, R., 1996. The NCEP/NCAR 40-Year Reanalysis Project. *Bull. Amer. Meteor. Soc.*, 77, 437–471. doi:dx.doi.org/10.1175/1520-0477(1996)077<0437:TNYRP>2.0.CO;2.

Kanamitsu, M., Ebisuzaki, W., Woollen, J., Yang, S.-K., Hnilo, J.J., Fiorino, M., Potter, G.L., 2002. NCEP-DOE AMIP-II Reanalysis (R-2). Bull. Amer. Meteor. Soc. 83, 1631–1643.

Kinder, T.H., Schumacher, J.D., 1981. Hydrographic structure over the continental shelf of the southeastern Bering Sea, in: Hood, D.W., Calder, J.A. (Eds.), The Eastern Bering Sea Shelf, Oceanography and Resources, vol. 1, Univ. of Wash. Press, Seattle, pp. 31–52.

Kinder, T.H., Chapman, D.C., Whitehead Jr, J.A., 1986. Westward intensification of the mean circulation on the Bering Sea shelf. J. Phys. Oceanogr. 16, 1217–1229.

Kowalik, Z., Stabeno, P., 1999. Trapped motion around the Pribilof Islands in the Bering Sea. J. Geophys. Res. 104(C11) 25,667–25,684, doi: 10.1029/1999JC900209.

Ladd, C., 2014. Seasonal and interannual variability of the Bering Slope Current. Deep-Sea Res. II 109, 5–13, doi:10.1016/j.dsr2.2013.12.005.

Ladd, C., Bond, N.A., 2002. Evaluation of the NCEP/NCAR reanalysis in the NE Pacific and the Bering Sea. J. Geophys. Res., 107 (C10), 3158, doi:10.1029/2001JC001157.

Luchin, V., Panteleev, G., 2014. Thermal regimes in the Chukchi Sea from 1941 to 2008. Deep Sea Res. II 109, 14–26, doi: 10.1016/j.dsr2.2014.05.007.

Moore, G.W.K., and Pickart, R.S., 2012. Northern Bering Sea tip jets. Geophys. Res. Lett. 39, L08807, doi:10.1029/2012GL051537.

Mordy, C.W., Stabeno, P.J., Ladd, C., Zeeman, S., Wisegarver, D.P., Salo, S.A., Hunt Jr., G., 2005. Nutrients and primary production along the eastern Aleutian Island Archipelago. Fish. Oceanogr. 14(Suppl. 1), 55–76, doi:10.1111/j.1365-2419.2005.00364.x.

Mordy, C.W., Eisner, L., Proctor, P., Stabeno, P.J., Devol, A., Shull, D.H., Napp, J.M., Whitledge, T., 2010. Temporary uncoupling of the marine nitrogen cycle:

Accumulation of nitrite on the Bering Sea Shelf. Mar. Chem. 121, 157–166, doi:10.1016/j.marchem.2010.04.004.

Mordy, C.W., Cokelet, E.D., Ladd, C., Menzia, F.A., Proctor, P., Stabeno, P.J., Wisegarver, E., 2012. Net community production on the middle shelf of the Eastern Bering Sea. Deep-Sea Res. II, 65–70, 110–125, doi:10.1016/j.dsr2.2012.02.012.

Reed, R.K., 1998. Confirmation of a convoluted flow over the southeastern Bering Sea shelf. Cont. Shelf Res. 18(1), 99–103, doi:10.1016/S0278-4343(97)00069-1.

Reed, R.K., Stabeno, P.J., 1999. The Aleutian North Slope Current, in: Loughlin, T.R., Ohtani, K. (Eds.), Dynamics of the Bering Sea: A Summary of Physical, Chemical, and Biological Characteristics, and a Synopsis of Research on the Bering Sea. University of Alaska Sea Grant, AK-SG-99-03, North Pacific Marine Science Organization (PICES), pp. 177–191.

Reid, J.L., 1986. On the total geostrophic circulation of the South Pacific Ocean: Flow patterns, tracers and transports. Prog. Oceanogr. 16(1), 1–61.

Schumacher, J.D., Kinder, T.H., 1983. Low-frequency current regimes over the Bering Sea shelf. J. Phys. Oceanogr. 13, 29,715–29,720, doi:10.1029/1999JC900242.

Schumacher, J.D., Stabeno, P.J., 1998. Continental shelf of the Bering Sea, Chapter 27 in in: Robinson, A.R., Brink, K.H. (Eds.), The Sea, Vol. 11, John Wiley and Sons, pp. 789–822.

Schumacher, J.D., Stabeno, P.J., Roach, A.T., 1989. Volume transport in the Alaska Coastal Current. Cont. Shelf Res. 9 (12), 1071–1083.

Stabeno, P.J., Hristova, H.G., 2014. Observations of the Alaskan Stream near Samalga Pass and its connection to the Bering Sea: 2001– 2004. Deep-Sea Res. I, 88, 30–46, doi: 10.1016/j.dsr.2014.03.002.

Stabeno, P.J., Reed, R.K., 1994. Circulation in the Bering Sea basin observed by satellite-tracked drifters: 1986–1993. J. Phys. Oceanogr. 24(4), 848–854.

Stabeno, P.J., Reed, R.K., Schumacher, J.D., 1995. The Alaska Coastal Current: Continuity of transport and forcing. J. Geophys. Res., 100(C2), 2477–2485, doi: 10.1029/94JC02842.

Stabeno, P.J., Bond, N.A., Kachel, N.B., Salo, S.A., Schumacher, J.D., 2001. On the temporal variability of the physical environment over the south-eastern Bering Sea. Fish. Oceanogr. 10(1), 81–98, doi:10.1046/j.1365-2419.2001.00157.x.

Stabeno, P.J., Reed, R.K., Napp, J.M., 2002. Transport through Unimak Pass, Alaska. Deep-Sea Res. Pt. II 49(26), 5919–5930, doi:10.1016/S0967-0645(02)00326-0.

Stabeno, P.J., Kachel, D.G., Kachel, N.B., Sullivan, M.E., 2005. Observations from moorings in the Aleutian Passes: Temperature, salinity and transport. Fish. Oceanogr., 14(Suppl. 1), 39–54, doi:10.1111/j.1365-2419.2005.00362.x.

Stabeno, P.J., Kachel, N., Mordy, C., Righi, D., Salo, S., 2008. An examination of the physical variability around the Pribilof Islands in 2004. Deep-Sea Res. II 55(16–17), 1701–1716, doi:10.1016/j.dsr2.2008.03.006.

Stabeno, P.J., Ladd, C., Reed, R.K., 2009. Observations of the Aleutian North Slope Current, Bering Sea, 1996–2001. J. Geophys. Res. 114, C05015, doi:10.1029/2007JC004705.

Stabeno, P.J., Napp, J., Mordy, C., Whitledge, T., 2010. Factors influencing physical structure and lower trophic levels of the eastern Bering Sea shelf in 2005: Sea ice, tides and winds. Prog. Oceanogr. 85(3–4), 180–196, doi:10.1016/j.pocean.2010.02.010.

Stabeno, P.J., E. Farley, N. Kachel, S. Moore, C. Mordy, J.M. Napp, J.E. Overland, A.I. Pinchuk, and M.F. Sigler, 2012a. A comparison of the physics of the northern and southern shelves of the eastern Bering Sea and some implications for the ecosystem. Deep-Sea Res. II, 65–70, doi: 10.1016/j.dsr2.2012.02.019, 14–30.

Stabeno, P.J., Kachel, N.B., Moore, S.E., Napp, J.M., Sigler, M., Yamaguchi, A., Zerbini, A.N., 2012b. Comparison of warm and cold years on the southeastern Bering Sea shelf and some implications for the ecosystem. Deep-Sea Res. II 65–70, 31–45, doi:10.1016/j.dsr2.2012.02.020.

Stabeno, P.J., Bell, S., Cheng, W., Danielson, S., Kachel, N.B., Mordy, C.W., in press. Long-term observations of Alaska Coastal Current in the northern Gulf of Alaska. Deep-Sea Res. II.

Stigebrandt, A., 1984. The North Pacific: A global-scale estuary. J. Phys. Oceanogr. 14, 464–470, doi:10.1175/1520-0485(1984)014<0464:TNPAGS>2.0.CO;2.

Stringer, W.J., Groves, J.E., 1991. Location and areal extent of polynyas in the Bering and Chukchi seas. Arctic 44, Supp. 1, 164–171.

Sullivan, M., Kachel, N.B., Mordy, C.W., Salo, S.A., Stabeno, P.J., 2014. Sea ice and water column structure on the eastern Bering Sea shelf. Deep-Sea Res. II 109, 39–56, doi: 10.1016/j.dsr2.2014.05.009.

Whitledge, T.E., Reeburgh, W.S., Walsh, J.J., 1986. Seasonal inorganic nitrogen distribution and dynamics in the southeastern Bering Sea. Cont. Shelf Res. 5, 109–132.

Wood, K.R., Bond, N.A., Danielson, S.L., Overland, J.E., Salo, S.A., Stabeno, P., Whitefield, J., 2014. A decade of environmental change in the Pacific–Arctic region. Prog. Oceanogr., in press, doi: 10.1016/j.pocean.2015.05.005.

Woodgate, R., Aagaard, K., 2005. Revising the Bering Strait freshwater flux into the Arctic Ocean. Geophys. Res. Lett. 32, L02602, doi:10.1029/2004GL021747.

Table 1. Listed below are the different mooring sites, their depths, positions, and deployment periods. The M2, M4, M5, and M8 moorings are long-term monitoring sites on the middle shelf and M3 was a site on the outer domain. UP is Unimak Pass; SB is Slime Bank; SG is St. George Island; PI is the Pribilof Islands; and IF is the inner front. The deployment period indicates the time when currents were measured at the mooring sites.

Mooring Site	Lat., Long. (°N), (°W)	Deployment period and comments
M1 (60 m)	55.07, 164.52	2/95-9/95
M2 (72 m)	56.87, 164.05	3/95-8/95,2/96-4/97,9/97-12.06,4/06-3/10,10/10-11/13
M3 (130 m)	56.05, 166.33	2/95-9/95, 2/96-9/96, 2/97-5/97, 5/98-9/98, 5/00-2/01
M4 (71 m)	57.85, 168.87	5/99-9/99, 5/00-4/05, 4/06-9/06, 4/07-4/09, 10/11-8/12
M5 (72 m)	59.90, 171.70	7/04-4/05,10/05-6/06,10/06-9/09,7/10-8/11,8/12-8/13
M8 (74 m)	62.20, 174.65	7/04-8/12
UP1 (76 m)	54.32, 164.77	3/80-8/80, 2/95-3/96, 9/96-9/97, 5/01-6/01, 5/02-8/02
SB1 (38 m)	55.10, 163.88	4/99-9/99
SB2 (60 m)	55.25, 163.95	4/99-9/99
SB3 (97 m)	55.42, 164.10	4/99-9/99
SG2 (200 m)	56.30, 169.33	6/97-4/98
SG3 (100 m)	56.47, 169.33	4/98-10/98, 4/99-9/99
PI3 (102 m)	57.12, 171.22	6/97-9/97, 5/98-9/98
PI5 (70 m)	57.13, 170.57	6/97-9/97, 5/98-9/98
IF1 (53 m)	58.67, 168.32	6/97-9/97, 5/98-9/98
IF2 (55 m)	58.67, 168.50	6/97-9/97, 5/98-12/98
IF3 (51 m)	58.72, 168.27	6/97-9/97, 5/98-12/98
IF4 (46 m)	58.83, 168.13	6/97-9/97, 5/98-9/98
IF5 (50 m)	58.70, 168.08	6/97-9/97, 5/98-9/98
IF6 (58 m)	58.55, 168.25	6/97-9/97, 5/98-9/98
IF7 (63 m)	58.48, 168.53	6/97-9/97, 5/98-9/98
IF8 (57 m)	58.63, 168.55	6/97-9/97, 5/98-9/98
IF9 (50 m)	58.80, 168.38	6/97-9/97, 5/98-9/98
CN (53 m)	57.41, 163.41	4/99-9/99

Table 2. Calculated geostrophic transports (referenced to the bottom) through Unimak Pass. Two estimates (indicated by *) used only three stations instead of the standard four stations (see inset Fig. 1). Here, summer is defined as May 15–September 30 and winter is defined as October 1–May 14.

Summer		Winter	
Date	Transport (10^6 m^3 s^{-1})	Date	Transport (10^6 m^3 s^{-1})
21 May 1995	0.19	23 Feb 1995	0.18
21 Aug 1995	0.31	15 Mar 1995	0.33
5 Sep 1995	0.51	21 Apr 1995	0.16
15 May 1996	0.04	4 May 1995	0.12
21 May 1996	0.27	25-26 Feb 1997	0.14
22 May 1996	0.08	25 Apr 1997	0.22
26 Sep 1997	0.13	11 May 1997	0.14
18-19 May	0.03	21 Feb 1998	0.17
18 May 2003	0.36	29 Apr 1998	-0.02
4 July 2008	0.06	6 Oct 1998	0.36
01 Sep 2008	0.13	25 Feb 2000	0.24
15 Jun 2009	0.09	21 Apr 2000	0.16
13 Jul 2010	0.06	30 Apr 2000	0.19
8 Sep 2010	-0.16	16 Feb 2002	0.06
		10 May 2005	0.41 *
		26 Feb 2007	0.29
		21 Apr 2007	-0.03*
		14 May 2008	0.08
Average± std	0.16±0.17		0.18±0.10

Table 3. Geostrophic transports referenced to the bottom on the St. Matthew Line (Fig. 1). Each of the ~10 stations used to calculate transport are indicated by “x” in Figure 1. The mean ± the standard deviation is given in the bottom line.

Cruise ID	Date	Transport (10^6 m^3 s^{-1})
TN179c	19 May 2005	0.30
HLY0701	23 Apr 2007	0.29
TN211	1 Oct 2007	0.33
HLY0802	7 Apr 2008	0.34
HLY0803	24 Jul 2008	0.28
ME0823	28 Aug 2008	0.23
HLY0902	10 Apr 2009	0.32
KM195-10	2 Jul 2009	0.29
MF00904b	5 Oct 2009	0.29
TN249	8 Jun 2010	0.42
TN250	3 Jul 2010	0.31
WE1008b	1 Sep 2010	0.37
Mean ± std		0.31± 0.05

Figure Captions

Figure 1. Map of the eastern Bering Sea shelf showing the place names and mooring sites (circles and squares) listed in Table 1 (e.g. IF, CN, M2). The multiple sites at IF, SB, SG and PI are indicated by smaller symbols. The vectors summarize the findings of this paper. The three primary currents on or near the southern shelf are: the 50-m isobath flow, the 100-m isobath flow, and the Aleutian North Slope Current/Bering Slope Current. Each hydrographic station in Unimak Pass (insert) and on the MN transect are indicated by "x".

Figure 2. Mean velocity at ~40 m calculated from the trajectories of ~ 500 satellite-tracked drifters. The dashed contour is the 100-m isobath and the solid contour is the 200-m isobath. The brown vectors in the north, each have less than 8 independent estimates of velocity.

Figure 3. a) Barotropic transport measured at the Unimak mooring (UP) site during the 6 years listed at top of panel. b) Barotropic transport (red) and total (black) transport measured at the Unimak Pass mooring site in 2002. Total transport was calculated using ADCP data.

Figure 4. Satellite-tracked drifter trajectories in the vicinity of Unimak Pass. The center of the drogue on each drifter was at ~40 m.

Figure 5. a) Near-surface currents (15 m) and b) near-bottom salinity and currents at M1. All time series have been low-pass filtered and velocities rotated 65°.

Figure 6. a) Along shelf transport perpendicular to the line of SB (Slime Bank) moorings east of Unimak Pass and b) salinity at 84 m at SB3.

Figure 7. Total transport along the 50-m isobath, perpendicular to the IF array (Fig. 1) near Nunivak Island in a) 1997 and b) 1998. The transect is ~55 km long.

Figure 8. a) Mean current vectors from the two-year 2008-2010 mooring deployments on the central shelf. Vector colors denote depth with red, yellow, green, blue, and black vectors at 5, 10, 20, and 30 m depths, respectively. At M5, pink indicates mean currents at 15 m, and purple indicates currents at 60 m. b) Mean currents for the IF mooring array in summers 1997 and 1998. Pink indicates mean currents at ~15 m depth and purple at ~10 m off the bottom. The box in (a) shows the location of the IF array shown in (b).

Figure 9. Transport was calculated on two transects across the 100-m isobath a) south of St. George Island and b) west of St. Paul Island. The transport south of St. George was westward and that west of St. Paul was northward.

Figure 10. Selection of trajectories of satellite-tracked drifters that transited the region north of the Pribilof Islands. a) These drifters (drogued at 40 m) were advected along the 100-m isobath south of St. George Island and continued along that isobath heading toward St. Matthew Island. b) These drifters were transiting in the BSC and were advected onto the shelf in Zhemchug Canyon.

Figure 11. Vertical sections of a) salinity, b) nitrate, and c) geostrophic flow referenced to the bottom along the hydrographic transect south of St. Matthew Island (MN in Fig. 1). This example (July 2010) is representative of other summer occupations.

Figure 12. Time scales of northward flow along a) the 100-m isobath and b) BSC and the northern part of the 100-m isobath. The black numerals indicate the number of months it takes a parcel to reach that point from its origin at a) Unimak Pass or b) Amukta Pass. The blue bars indicate where a parcel of water would intercept the ice. For example in (b), “Sep” indicates where the parcel starting at the origin (Amukta Pass) on September 1 would intercept the ice ~between 5 and 6 months later. Similarly, parcel starting in Amukta Pass in May would intercept the ice between 7 and 8 months later.

Figure 13. Monthly mean near-surface (~12-17 m) and near-bottom (~60 m) currents measured at a) M8, b) M5, c) M4, and d) M2. The magenta vectors indicate near surface flow and the black vectors indicate near bottom flow.

Figure 14. Monthly mean vectors divided into warm years (red) and cold years (blue). a) near-surface (~12-17 m) measurements and b) near-bottom (~60 m) measurements at M4; and c) near-surface measurements and d) near-bottom measurements at M2. Warm years were 1998, 2001–2005 and cold years were 1995, 1997, 1999, 2007–2010, 2012-2013. The remaining years were average (Stabeno et al., 2012b).

Figure 15. Relationship between winds and currents at M2. The period examined is winter when there is no ice for a) near-surface (~12-17 m), b) near-bottom (~60 m), and c) the difference between near-surface and near-bottom. In the left column, vectors indicate the mean direction of the flow when the winds are toward the octant indicated (e.g., 270°-315°). Right column shows current direction as a function of wind direction (black line) and the number of points in each direction octant (shaded). The red lines are at 45° and 90° to the right of the wind.

Figure 16. Monthly mean near-bottom currents and daily near-bottom salinity (red) at M5. The blue lines indicate the presence sea ice (areal coverage > 30%).

Figure 17. Relationship between winds and currents at M8. The period examined is winter when there is no ice for a) near-surface (~12-17 m), and b) the difference between near-surface and near-bottom flow. In the top panels, vectors indicate the mean direction of the flow when the winds are toward the octant indicated (e.g., 270°-315°). The bottom panels show current direction as a function of wind direction (black line) and the number of points in each direction octant (shaded). The red lines are at 45° and 90° to the right of the wind.

Figure 18. a) Average annual salinity at M2 (1995–2013). b) The percentage of water flushed from the shelf during late October–February 1 for four different values of slope

salinity. Note that the salinities in October 1996, when water column became well mixed at M2, and January 1997, when ice arrived, were identical, which indicates there was little or no replenishment that year.

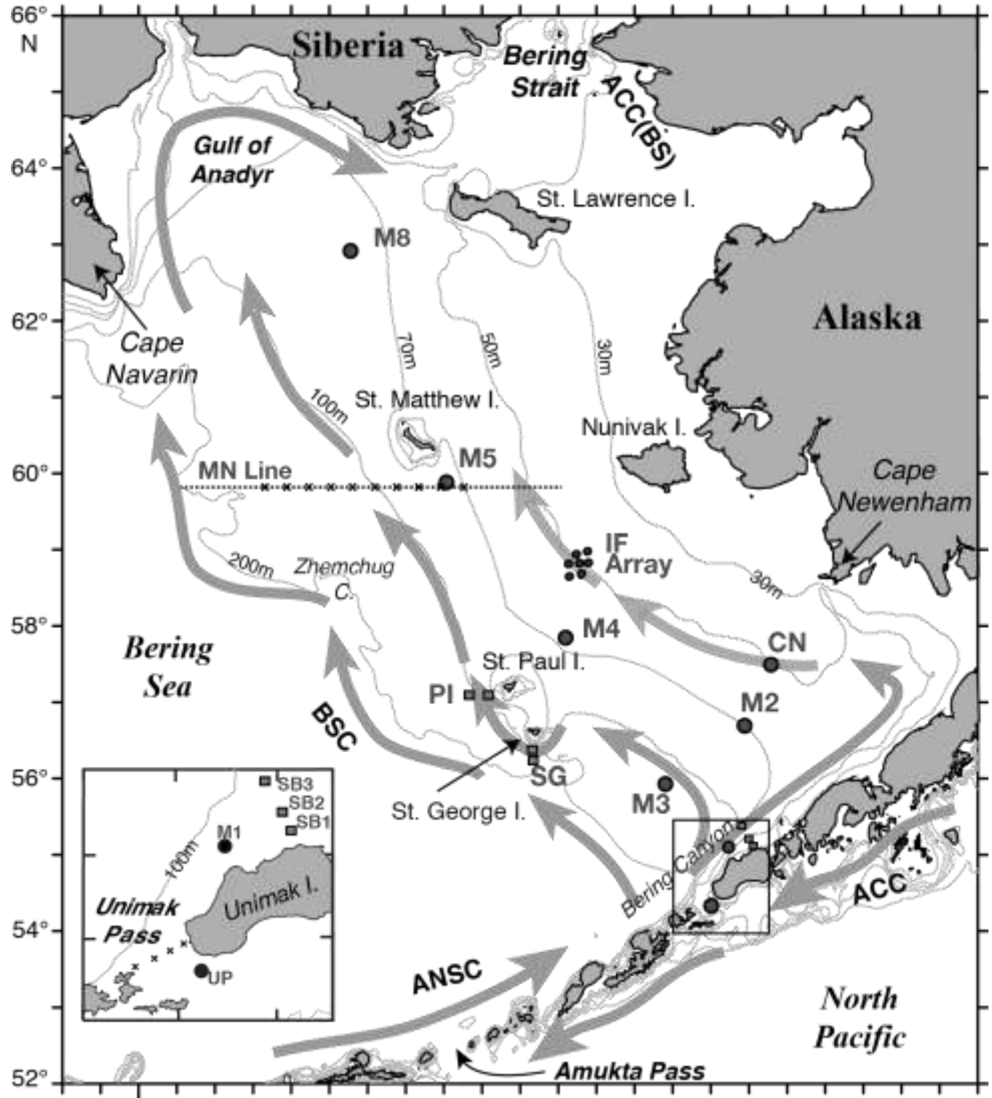

Figure 1. Map of the eastern Bering Sea shelf showing the place names and mooring sites listed in Table 1 (e.g. IF, CN, M2). The vectors summarize the findings of this paper. The three primary currents on or near the southern shelf are: the 50-m isobath flow, the 100-m isobath flow, and the Aleutian North Slope Current/Bering Slope Current. Each hydrographic station in Unimak Pass (insert) and on the MN transect are indicated by "x".

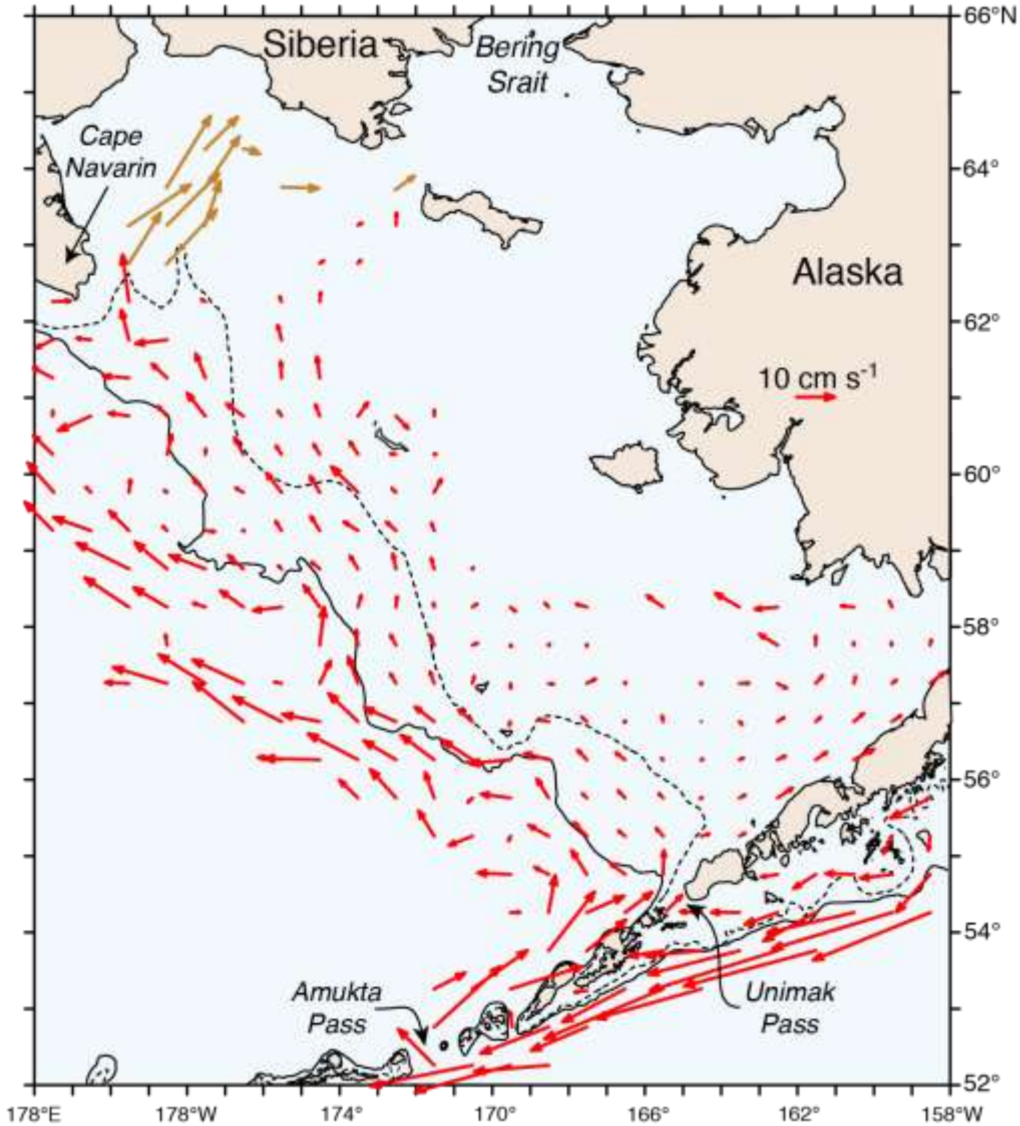

Figure 2. Mean velocity at ~40 m calculated from the trajectories of ~ 500 satellite-tracked drifters. The dashed contour is the 100-m isobath and the solid contour is the 200-m isobath. The brown vectors in the north, each have less than 8 independent estimates of velocity.

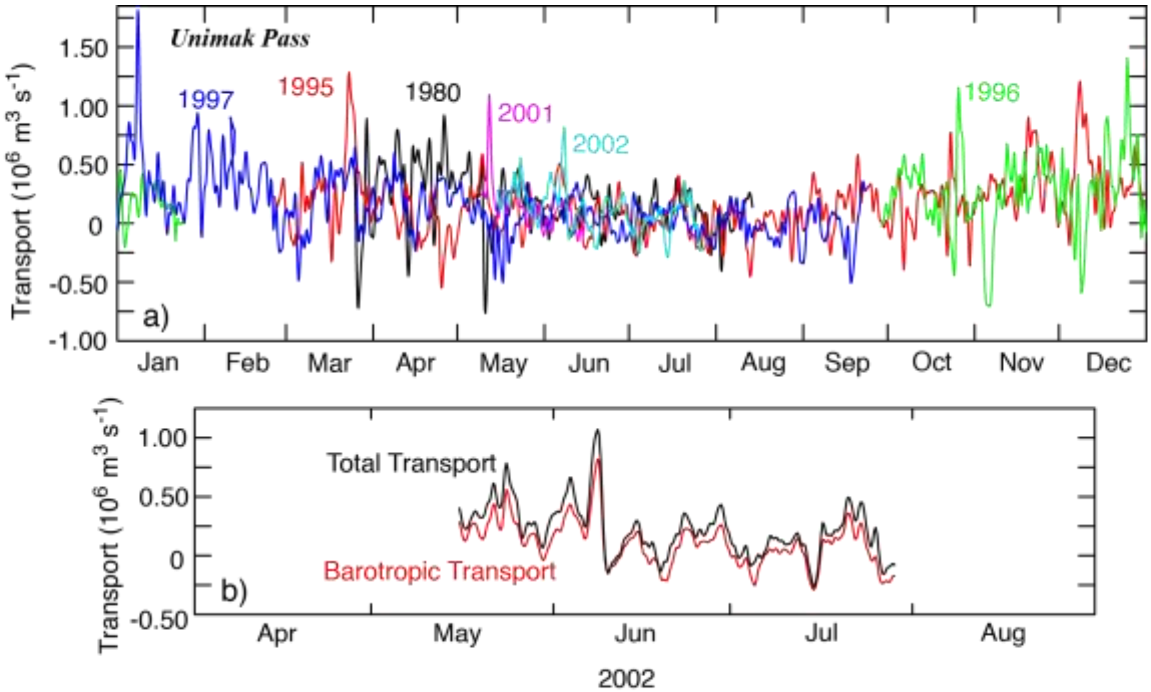

Figure 3. a) Barotropic transport measured at the Unimak mooring (UP) site during the 6 years listed at top of panel. b) Barotropic transport (red) and total (black) transport measured at the Unimak Pass mooring site in 2002. Total transport was calculated using ADCP data.

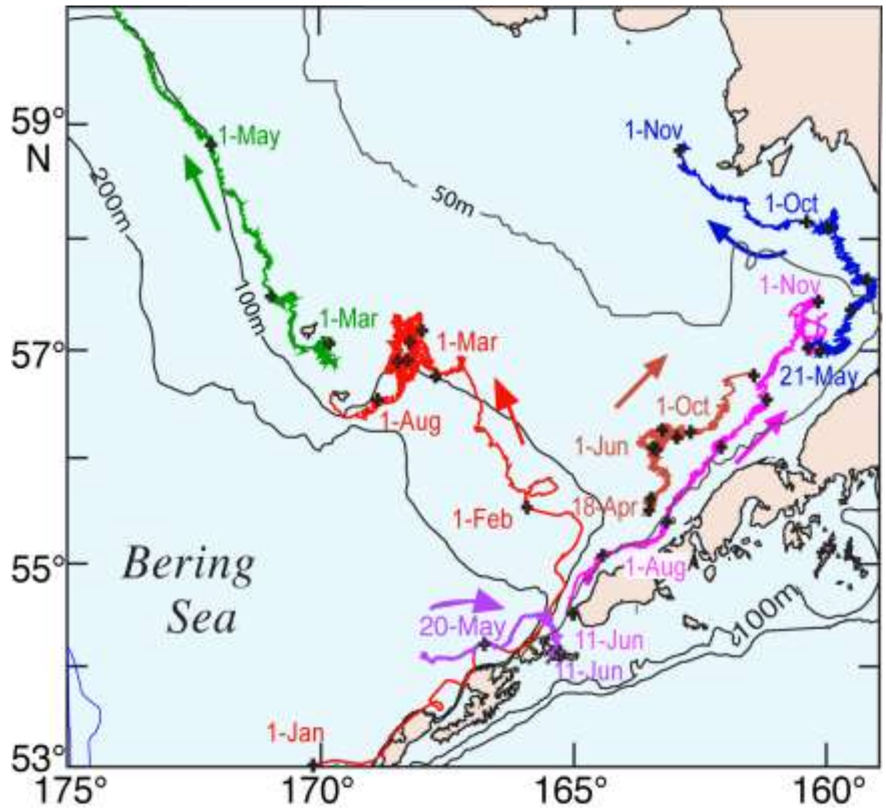

Figure 4. Satellite-tracked drifter trajectories in the vicinity of Unimak Pass. The center of the drogue on each drifter was at ~40 m.

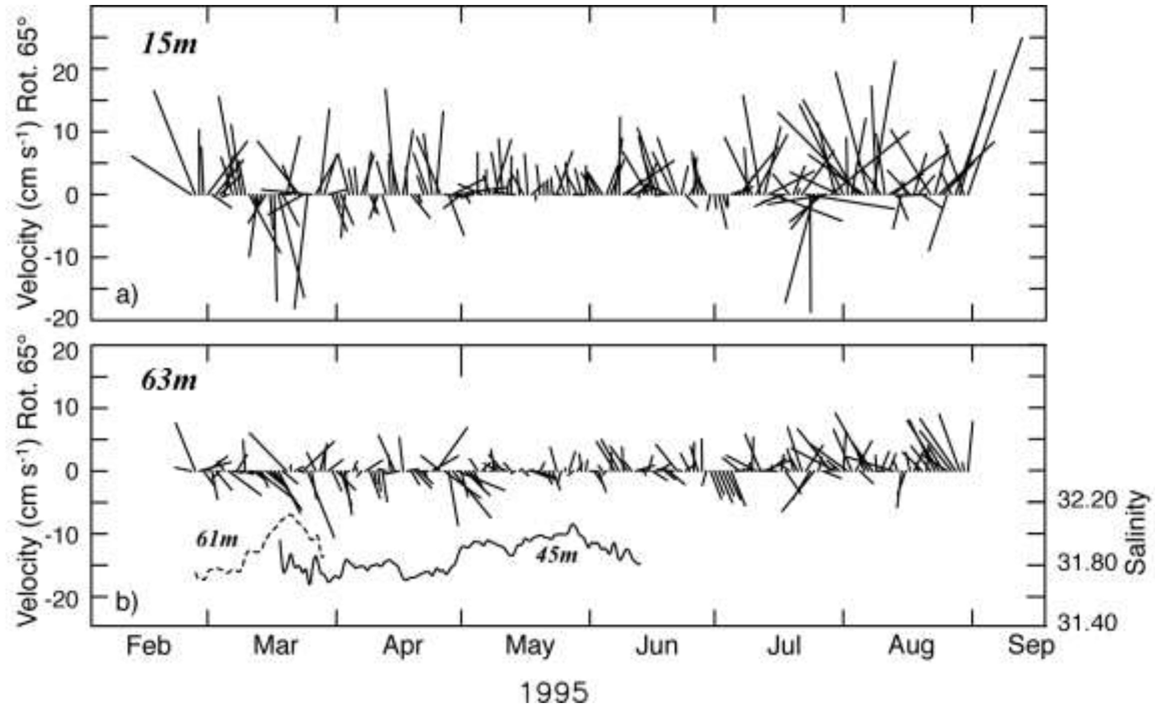

Figure 5. a) Near-surface currents (15 m) and b) near-bottom salinity and currents at M1. All time series have been low-pass filtered and velocities rotated 65°.

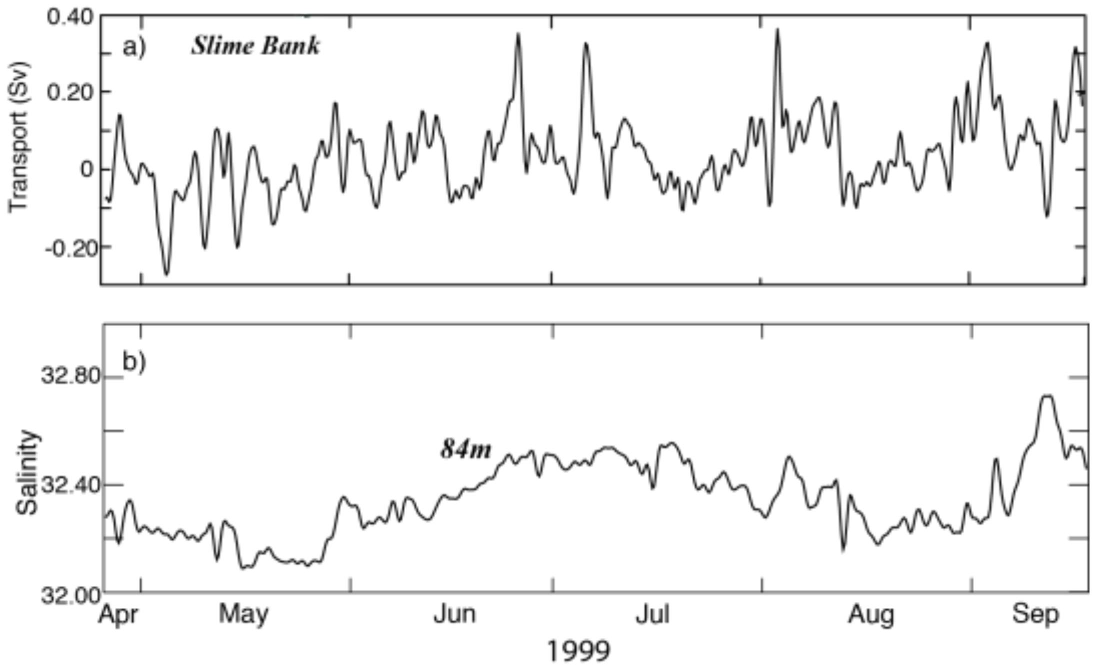

Figure 6. a) Along shelf transport perpendicular to the line of SB (Slime Bank) moorings east of Unimak Pass and b) salinity at 84 m at SB3.

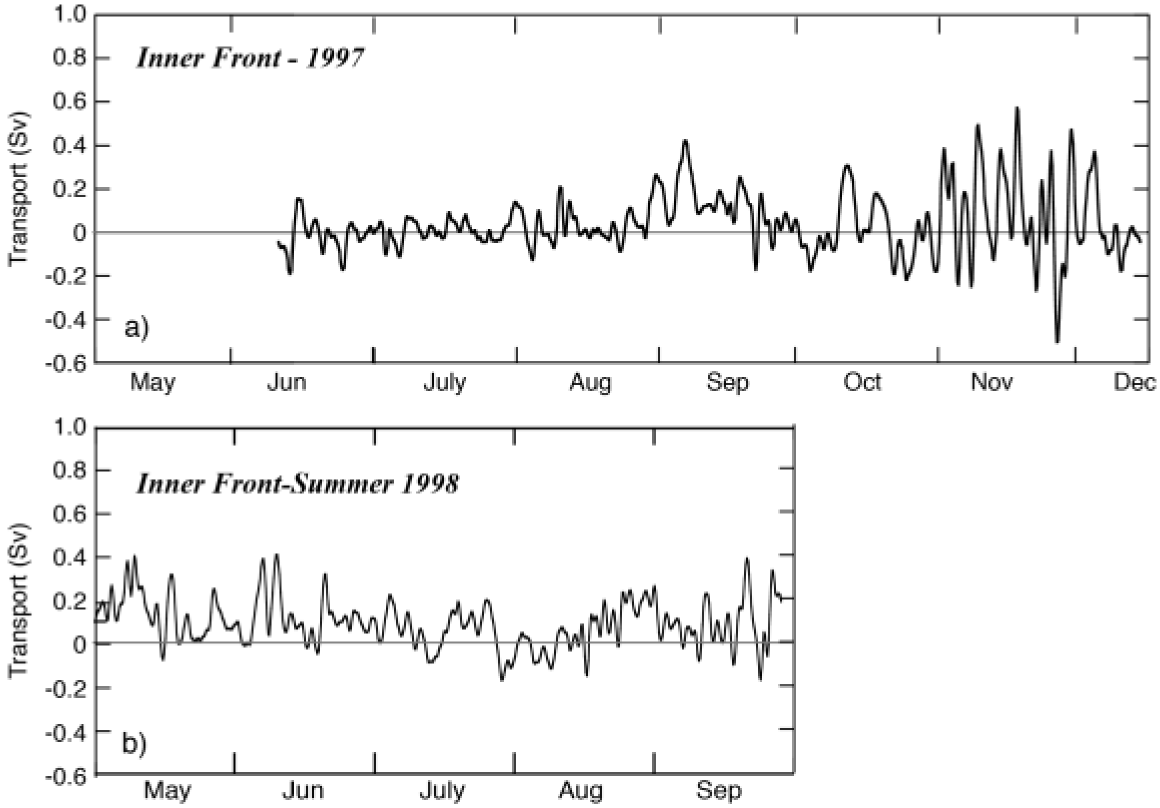

Figure 7. Total transport along the 50-m isobath, perpendicular to the IF array (Fig. 1) near Nunivak Island in a) 1997 and b) 1998. The transect is ~55 km long.

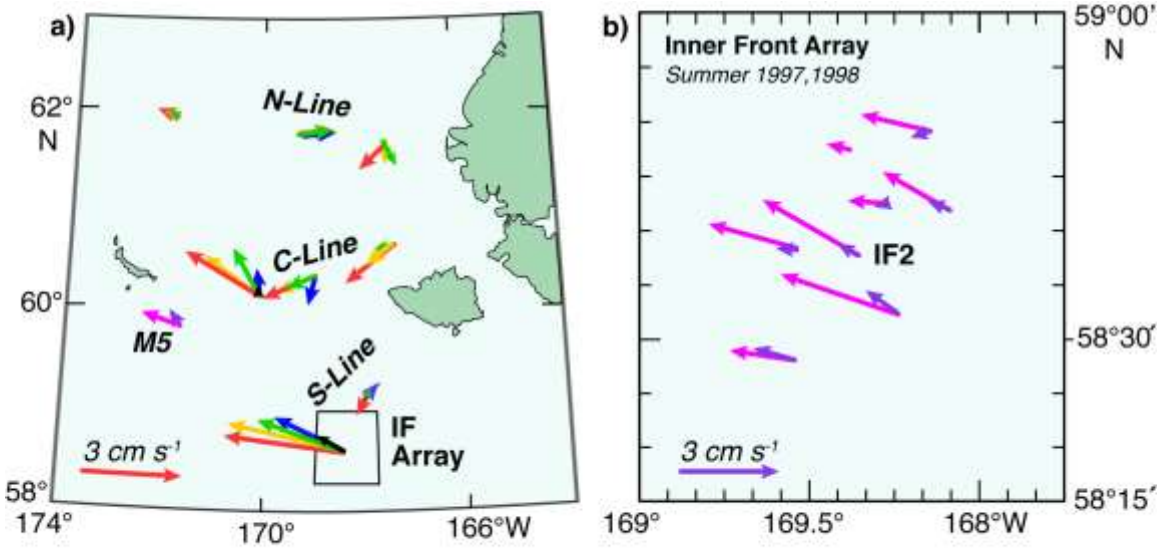

Figure 8. a) Mean current vectors from the two-year 2008-2010 mooring deployments on the central shelf. Vector colors denote depth with red, yellow, green, blue, and black vectors at 5, 10, 20, and 30 m depths, respectively. At M5, pink indicates mean currents at 15 m, and purple indicates currents at 60 m. b) Mean currents for the IF mooring array in summers 1997 and 1998. Pink indicates mean currents at ~15 m depth and purple at ~10 m off the bottom. The box in (a) shows the location of the IF array shown in (b).

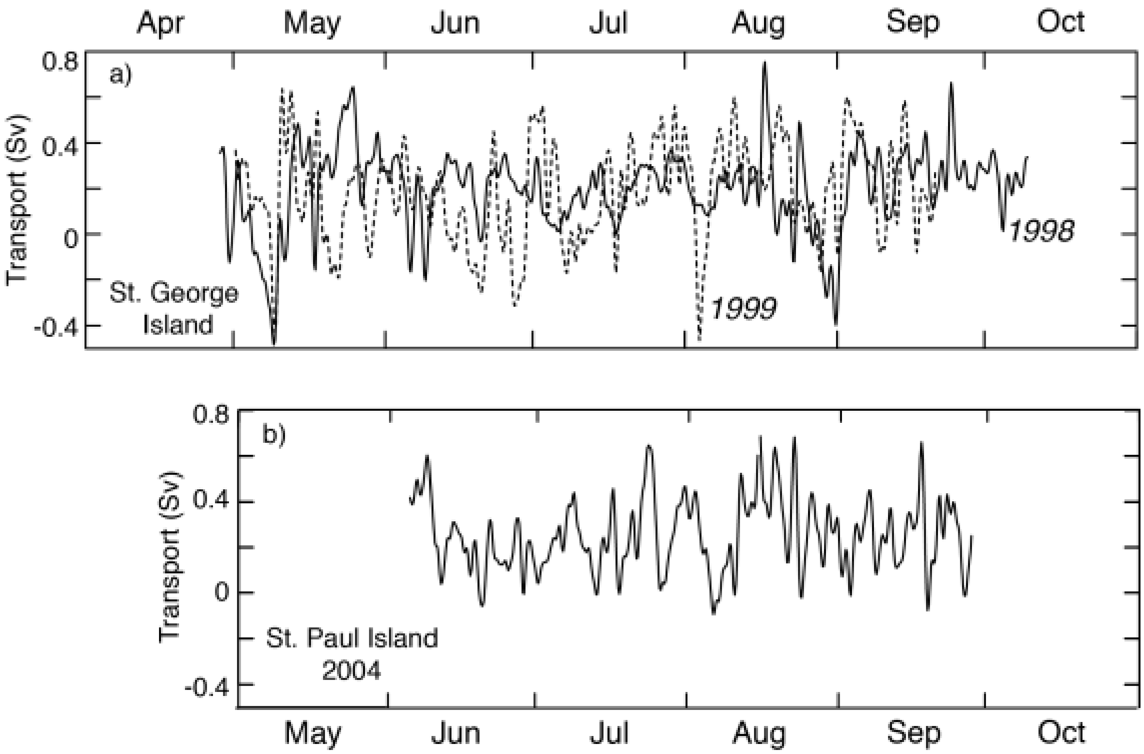

Figure 9. Transport was calculated on two transects across the 100-m isobath a) south of St. George Island and b) west of St. Paul Island. The transport south of St. George was westward and that west of St. Paul was northward.

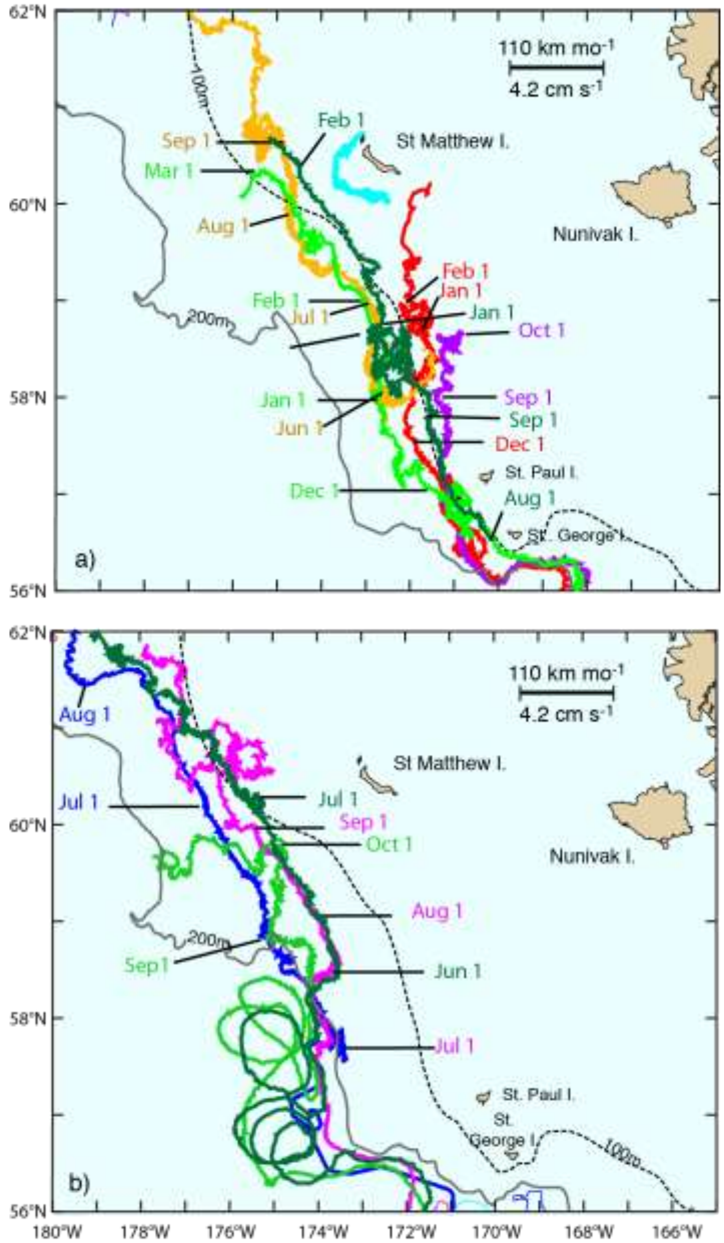

Figure 10. Selection of trajectories of satellite-tracked drifters that transited the region north of the Pribilof Islands. a) These drifters (drogued at 40 m) were advected along the 100-m isobath south of St. George Island and continued along that isobath heading toward St. Matthew Island. b) These drifters were transiting in the BSC and were advected onto the shelf in Zhemchug Canyon.

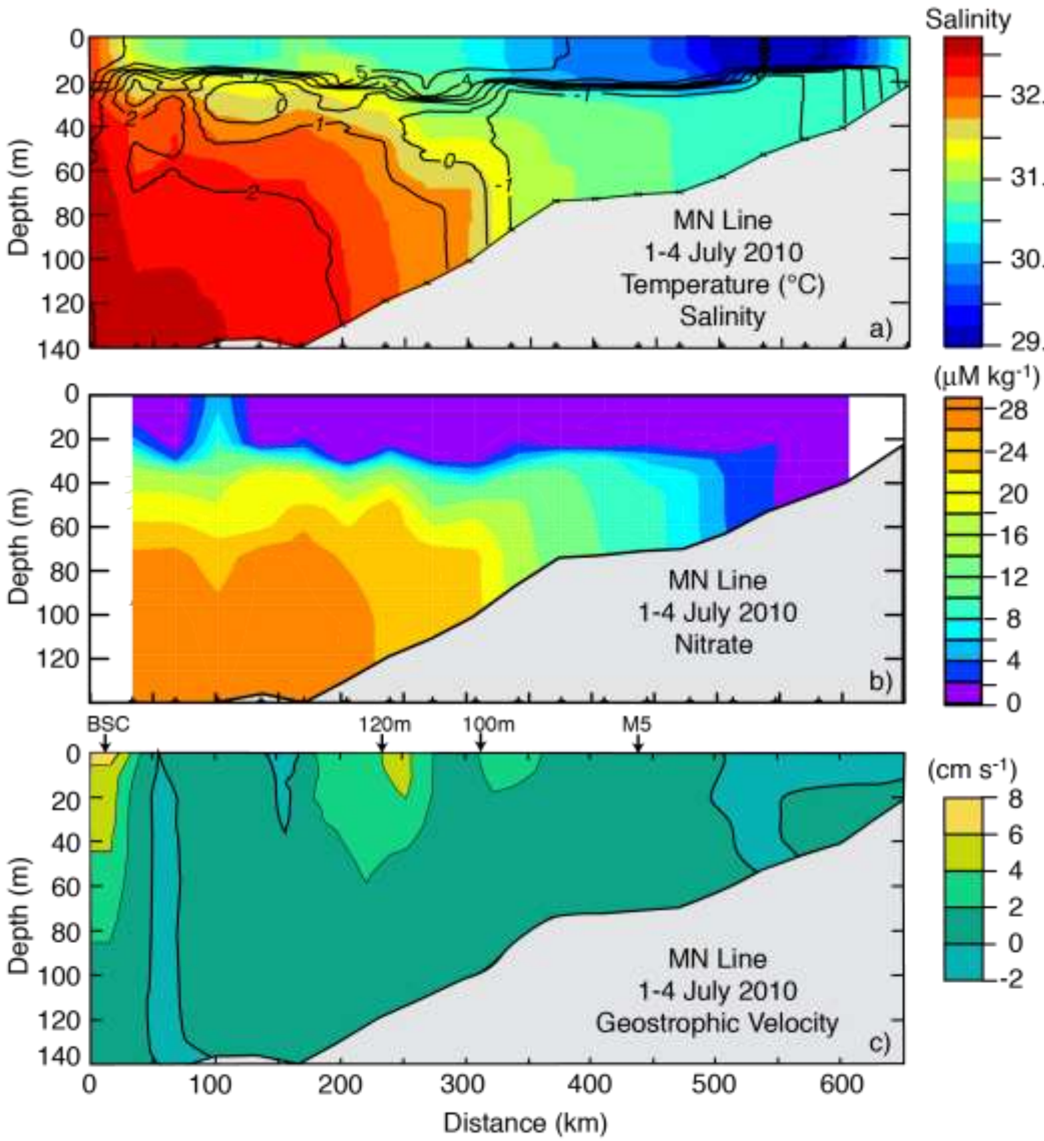

Figure 11. Vertical sections of a) salinity, b) nitrate, and c) geostrophic flow referenced to the bottom along the hydrographic transect south of St. Matthew Island (MN in Fig. 1). This example (July 2010) is representative of other summer occupations.

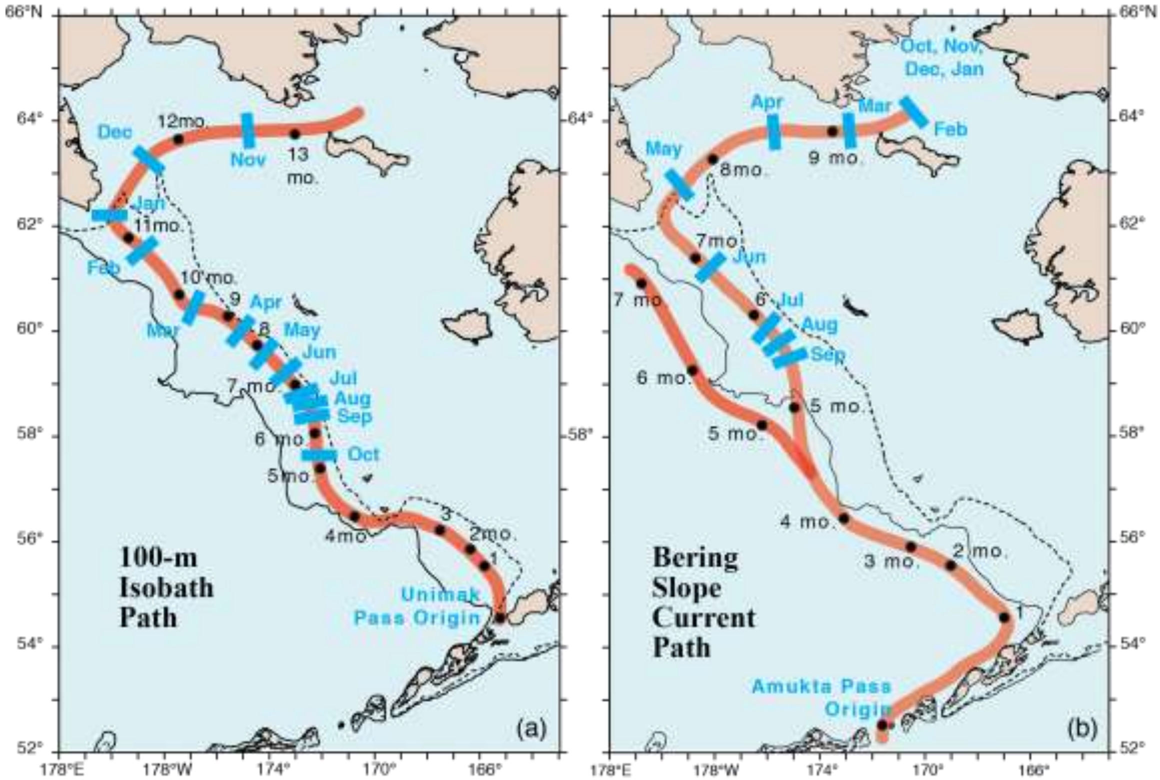

Figure 12. Time scales of northward flow along a) the 100-m isobath and b) BSC and the northern part of the 100-m isobath. The black numerals indicate the number of months it takes a parcel to reach that point from its origin at a) Unimak Pass or b) Amukta Pass. The blue bars indicate where a parcel of water would intercept the ice. For example in (b), “Sep” indicates where the parcel starting at the origin (Amukta Pass) on September 1 would intercept the ice ~between 5 and 6 months later. Similarly, parcel starting in Amukta Pass in May would intercept the ice between 7 and 8 months later.

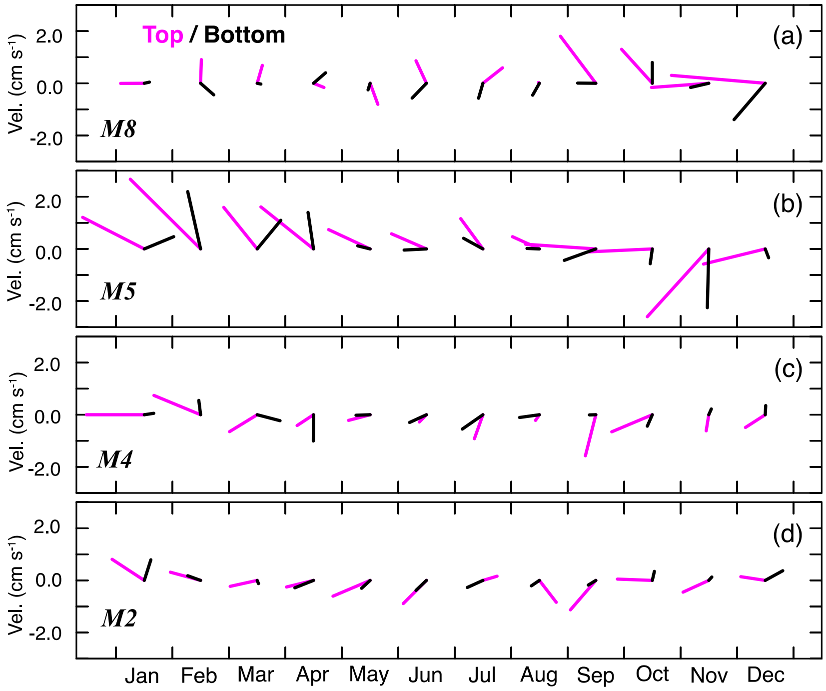

Figure 13. Monthly mean near-surface (~12-17 m) and near-bottom (~60 m) currents measured at a) M8, b) M5, c) M4, and d) M2. The magenta vectors indicate near surface flow and the black vectors indicate near bottom flow.

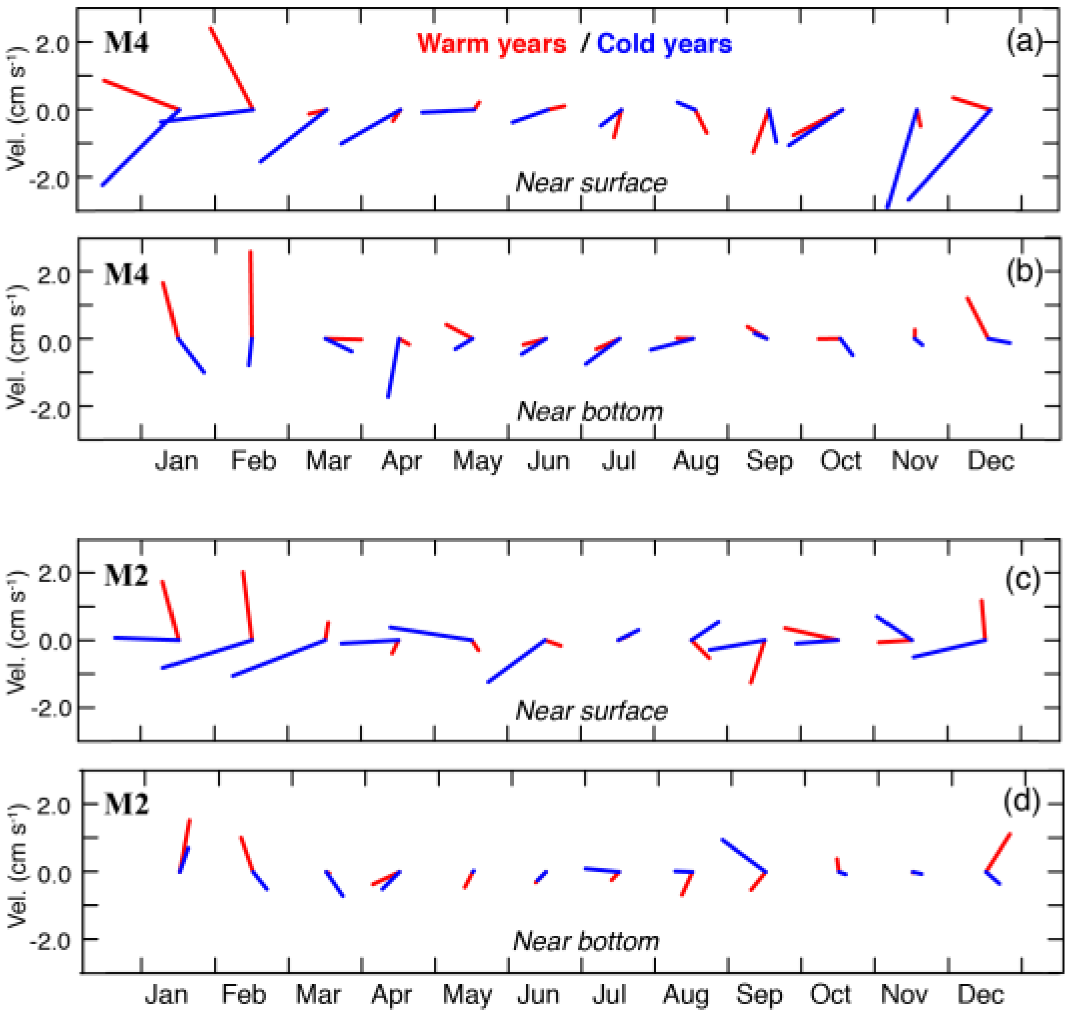

Figure 14. Monthly mean vectors divided into warm years (red) and cold years (blue). a) near-surface (~12-17 m) measurements and b) near-bottom (~60 m) measurements at M4; and c) near-surface measurements and d) near-bottom measurements at M2. Warm years were 1998, 2001–2005 and cold years were 1995, 1997, 1999, 2007–2010, 2012-2013. The remaining years were average (Stabeno et al., 2012b).

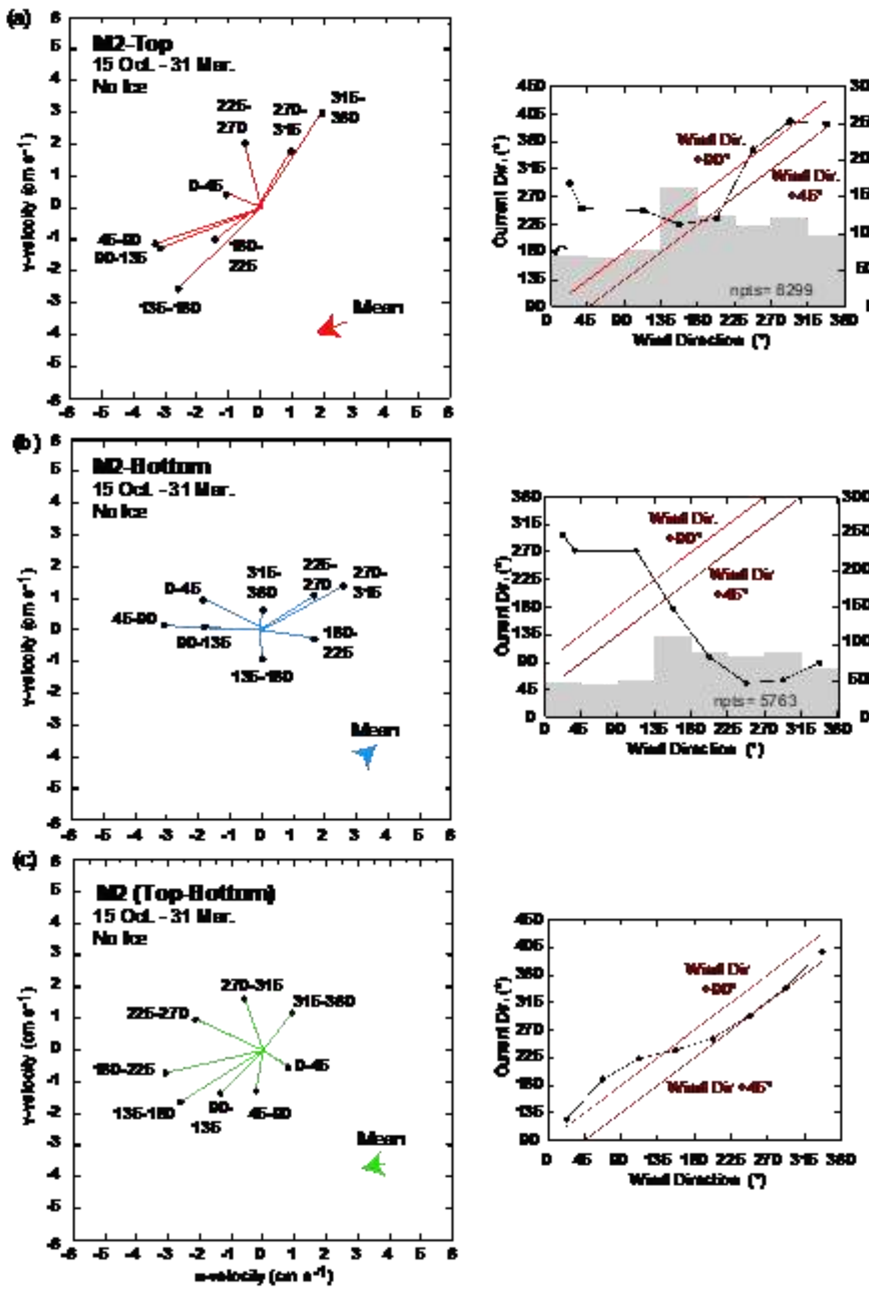

Figure 15. Relationship between winds and currents at M2. The period examined is winter when there is no ice for a) near-surface (~12-17 m), b) near-bottom (~60 m), and c) the difference between near-surface and near-bottom. In the left column, vectors indicate the mean direction of the flow when the winds are toward the octant indicated (e.g., 270°-315°). Right column shows current direction as a function of wind direction (black line) and the number of points in each direction octant (shaded). The red lines are at 45° and 90° to the right of the wind.

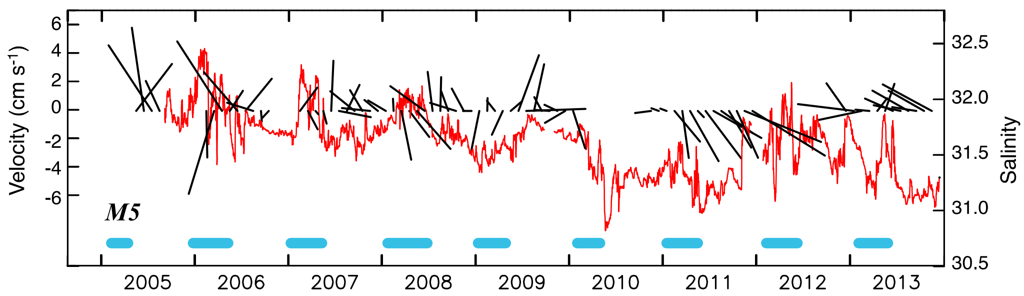

1166

1167 Figure 16. Monthly mean near-bottom currents and daily near-bottom salinity (red) at

1168 M5. The blue lines indicate the presence sea ice (areal coverage > 30%).

1169

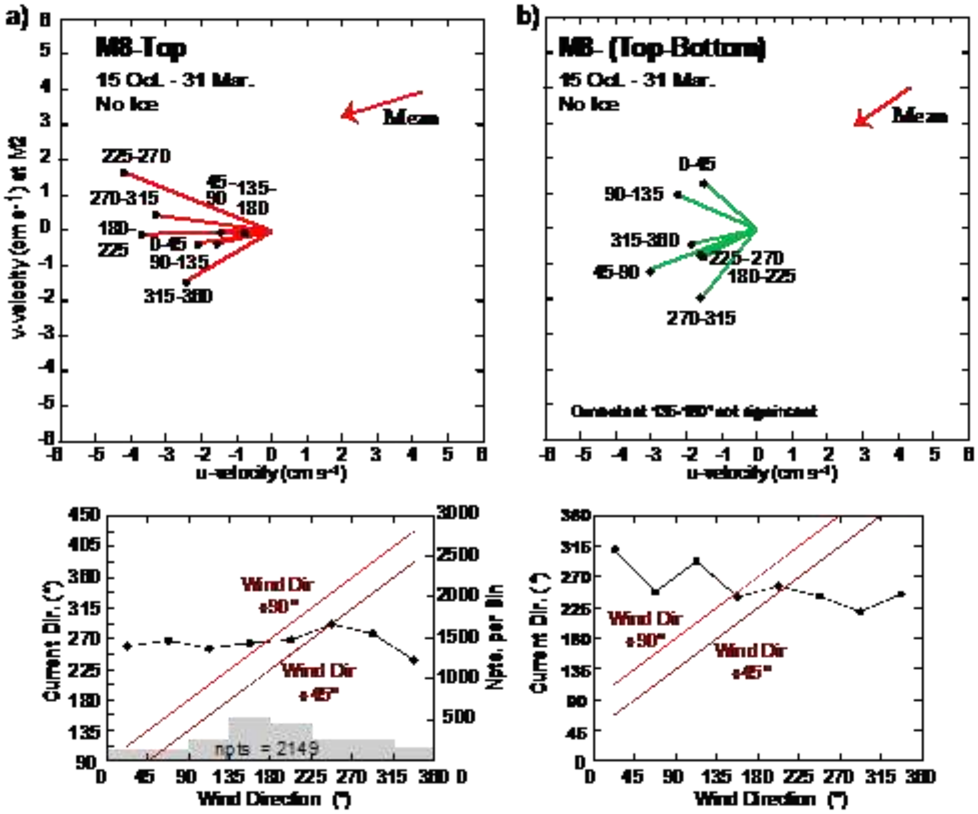

Figure 17. Relationship between winds and currents at M8. The period examined is winter when there is no ice for a) near-surface (~12-17 m), and b) the difference between near-surface and near-bottom flow. In the top panels, vectors indicate the mean direction of the flow when the winds are toward the octant indicated (e.g., 270°-315°). The bottom panels show current direction as a function of wind direction (black line) and the number of points in each direction octant (shaded). The red lines are at 45° and 90° to the right of the wind.

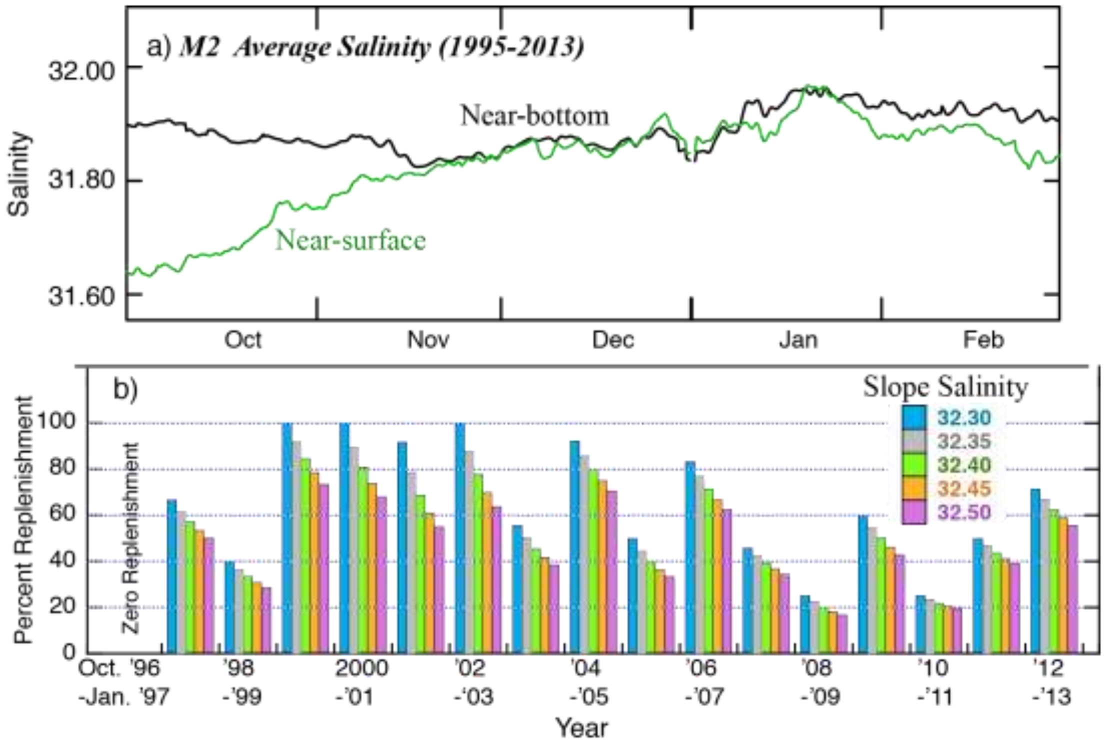

Figure 18. a) Average annual salinity at M2 (1995–2013). b) The percentage of water flushed from the shelf during late October–February 1 for four different values of slope salinity. Note that the salinities in October 1996, when water column became well mixed at M2, and January 1997, when ice arrived, were identical, which indicates there was little or no replenishment that year.